

Review

A Review of Techniques and Bio-Heat Transfer Models Supporting Infrared Thermal Imaging for Diagnosis of Malignancy

Giampaolo D'Alessandro ¹, Pantea Tavakolian ² and Stefano Sfarra ^{1,*}

¹ Department of Industrial and Information Engineering and Economics, University of L'Aquila, 67100 L'Aquila, Italy; giampaolo.dalessandro@univaq.it

² Biomedical Engineering Program, College of Engineering & Mines, University of North Dakota, Grand Forks, ND 58202, USA; pantea.tavakolian@und.edu

* Correspondence: stefano.sfarra@univaq.it

Abstract: The present review aims to analyze the application of infrared thermal imaging, aided by bio-heat models, as a tool for the diagnosis of skin and breast cancers. The state of the art of the related technical procedures, bio-heat transfer modeling, and thermogram post-processing methods is comprehensively reviewed. Once the thermal signatures of different malignant diseases are described, the updated thermographic techniques (steady-state and dynamic) used for cancer diagnosis are discussed in detail, along with the recommended best practices to ensure the most significant thermal contrast observable between the cancerous and healthy tissues. Regarding the dynamic techniques, particular emphasis is placed on innovative methods, such as lock-in thermography, thermal wave imaging, and rotational breast thermography. Forward and inverse modeling techniques for the bio-heat transfer in skin and breast tissues, supporting the thermographic examination and providing accurate data for training artificial intelligence (AI) algorithms, are reported with a special focus on real breast geometry-based 3D models. In terms of inverse techniques, different data processing algorithms to retrieve thermophysical parameters and growth features of tumor lesions are mentioned. Post-processing of infrared images is also described, citing both conventional processing procedures and applications of AI algorithms for tumor detection.

Keywords: bio-heat transfer; infrared thermal imaging; inverse modeling; steady-state and dynamic thermography; post-processing images; skin cancer; breast cancer



Citation: D'Alessandro, G.; Tavakolian, P.; Sfarra, S. A Review of Techniques and Bio-Heat Transfer Models Supporting Infrared Thermal Imaging for Diagnosis of Malignancy. *Appl. Sci.* **2024**, *14*, 1603. <https://doi.org/10.3390/app14041603>

Academic Editor: Vladislav Toronov

Received: 25 December 2023

Revised: 10 February 2024

Accepted: 13 February 2024

Published: 17 February 2024



Copyright: © 2024 by the authors. Licensee MDPI, Basel, Switzerland. This article is an open access article distributed under the terms and conditions of the Creative Commons Attribution (CC BY) license (<https://creativecommons.org/licenses/by/4.0/>).

1. Introduction

Breast cancer was the most common cancer worldwide in 2022, with more than 2.26 million new diagnoses in women in 2020, whereas melanoma of the skin was the 17th most common cancer, with more than 150,000 new cases [1]. As far as non-melanoma skin cancers are concerned, they are under-reported in the national cancer registry data as they are very common, often under-diagnosed, and commonly treated within primary care. For these reasons, they are often excluded from the reporting of cancer statistics [1]. Additionally, it was estimated that in the EU 27 countries, melanoma accounted for 4% of all new cancer diagnoses (all cancers, excluding non-melanoma skin cancers), with about 16,500 deceased subjects in 2020 [2]. In the same countries, breast cancer was the most diagnosed cancer (13.8%) in 2022 [2], and it claimed 95,800 lives in the same year [2].

Early diagnostic tools could significantly increase survival rates and reduce health-care costs. Apart from invasive examination (biopsy), the visual inspection-based ABCDE criteria are commonly used by expert dermatologists for skin lesions diagnosis as well as dermoscopy. However, at very early stages, melanomas may resemble benign lesions [3,4] and, therefore, visual inspection can sometimes be inaccurate. In regard to breast cancer diagnosis, mammography is considered the gold standard. Notwithstanding, it suffers from low sensitivity for dense breasts in younger women, exposure to X-ray radiation, and

relatively high costs [5]. Developing new, accurate, objective, and early diagnostic tools is essential not only to overcome these limitations but also to avoid unnecessary biopsies and consequently reduce the costs of national health-care systems.

Infrared (IR) thermography is one of the most promising technologies now available for the early detection of malignant diseases (such as skin and breast cancers). Its significant strengths are the absence of contact and dangerous radiation; it is also a non-invasive and cost-effective technique. It is based on identifying abnormal thermal patterns on the observed skin surface when compared to the healthy region, as they are recognized as biological risk markers [6]. Surprisingly, the first applications of IR thermography to diagnose breast cancers and melanomas date back to 1956 [7] and 1969 [8], respectively. However, when the observed differences between thermal patterns of cancerous and healthy tissues were subtle, this methodology showed drawbacks and limits due to poor resolution and the scan time of the first IR cameras. Moreover, the absence of standardized measurement procedures and the lack of clinicians adequately trained in the use of IR cameras represented other obstacles to the development of such a methodology. Because of these problems, IR thermography did not become popular as a diagnostic tool [6,9–12], although in 1982, it was approved as an adjunctive tool for the diagnosis of breast cancer by the Food and Drug Administration in the USA [5]. Later in the 2000s, the performance of IR cameras was significantly improved thanks to the introduction of high-sensitivity uncooled IR detectors (known as focal plane arrays), allowing less pronounced surface temperature variations to be detected. As a consequence of the improvement in IR cameras' performance along with the increasing computational capability (crucial for both realistic models and artificial intelligence algorithms), IR thermography has gained a renewed interest as a diagnostic tool. Furthermore, the increasing computational capability allows for more accurate numerical models, which are able to predict the complex relationship between surface thermal patterns and the underlying pathophysiological conditions, to be implemented and used both as support for thermographic examination and to provide reliable data useful for training artificial intelligence algorithms. Additionally, relevant information about thermophysical parameters and growth features of tumor lesions can be inferred from surface temperature distributions using inverse techniques.

To the best of the authors' knowledge, other reviews on this topic are devoted to specific aspects of IR thermography applied for the diagnosis of a particular kind of cancer. Examples are the reviews dedicated to breast cancer detection authored by Kandlikar et al. [13] and by Mashekova et al. [14]. The former addresses both the general aspects of thermography and numerical simulations, highlighting the need for realistic models, while the latter discusses mainly the geometrical aspects of thermal modeling and computer-aided diagnostic tools, underlining the applications of artificial intelligence algorithms. Additionally, the review offered by Ng [6] discusses the camera performance and the environmental requirements, enabling the use of IR thermography as a tool for breast tumor screening. As far as skin cancer detection is concerned, the work by Akther et al. [4] briefly reviews the experimental studies aimed at detecting melanoma, while the review by Verstockt et al. [15] provides an overview of measurement set-ups and technical procedures used for skin cancer diagnosis.

Contrarily to these review papers, the present review has the goal of comprehensively describing the state of the art of technical procedures, bio-heat transfer modeling, and thermogram post-processing methods, aiding IR thermal imaging for the diagnosis of both skin cancers and breast tumors.

This review paper is organized as follows: Section 2 describes the thermal signatures of different malignant diseases observable through IR thermography. The updated thermographic techniques used for the diagnosis of skin cancers and breast tumors are reviewed in Sections 3 and 4, respectively. Steady-state techniques for skin cancer diagnosis are handled in Section 3.1, while the related dynamic techniques are treated in Section 3.2, in which classical dynamic IR thermography (along with the cold stimuli applied on the skin surface), lock-in thermography, and frequency-modulated thermal wave imaging method

are highlighted. Regarding the thermographic techniques for breast cancer diagnosis, apart from the stationary ones (Section 4.1), particular emphasis is placed on the dynamic techniques (Section 4.2), with a special focus on rotational breast thermography.

Forward multi-layer models for the bio-heat transfer in skin tissues are described in Section 5.1, while inverse modeling techniques, such as least squares minimization-based methods and alternative algorithms, are handled in Section 5.2. Section 6 is devoted to forward (Section 6.1) and inverse (Section 6.2) modeling of breast tissues. Real breast geometry-based models are particularly mentioned. Finally, thermogram post-processing methods, related to the application of both classical processing procedures and artificial intelligence algorithms for the diagnosis of skin and breast cancers, are discussed in Section 7.

2. Thermal Signature of Malignancy

2.1. Skin Cancers

Skin cancers (also known as skin neoplasms) are generally classified based on the kind of skin cell from which they arise. Basal cell carcinoma (BCC), squamous cell carcinoma (SCC), and melanoma (a malignant transformation of melanocytes) are the most common skin cancers by the number of diagnosed cases. Each type of these skin neoplasms exhibits a characteristic thermal signature, as shown by Gonzalez et al. [16]. These authors examined 30 patients with a reported diagnosis of melanoma (in 6 cases) and non-melanoma (18 BCC and 6 SCC) skin neoplasms using an FLIR T400 IR camera (320 × 240 Focal Plane Array, with a spectral range of 7.5–13 μm and a thermal sensitivity of 50 mK at 30 °C). Based on the acquired thermal images, they found that BCCs show negative temperature differences between the cancer lesion and the healthy skin, while SCCs and melanomas exhibit positive differences instead [16]. These thermal signatures were also studied in relation to the vascularity of the skin lesion. In particular, for BCCs, a strong correlation between local temperature lesion and vascularity was found, suggesting a low metabolic heat production due to the tumor with respect to the variation of its vascularity; for SCCs, the results showed that there is a constant ratio between metabolic heat production and vascularity; while for melanomas, the local temperature increases even though the vascularity of the tumor does not increase, suggesting that there is a higher variation in metabolic heat produced by the tumor [16]. These conclusions are not only useful to correctly identify different kinds of skin cancers through thermal imaging, but they also provide further information for thermal modeling of skin neoplasms.

2.2. Breast Cancers

The important role of infrared thermography in assessing the risk of breast cancer was revealed thanks to the study carried out by Head et al. [17] in 2000. These authors, using second-generation focal-plane indium-antimonide IR detector systems, demonstrated that women with abnormal IR breast images had an increased risk of about 30% of developing breast cancer. They also showed the prognostic value of IR thermography for breast cancer patients. Indeed, at that time, they found that 65% of the examined subjects with a breast cancer diagnosis had abnormal IR images within the one-year period leading up to their diagnosis, while 88% of the patients who died of breast cancer had abnormal IR images during the same period.

Invasive ductal carcinoma (IDC), ductal carcinoma in situ (DCIS), and invasive lobular carcinoma (ILC) are the three most common types of breast cancers [18]. Each of them affects specific cells of the mammary tissue. In particular, DCIS affects the cells lining the ducts, whereas when the walls of the ducts are involved, IDC occurs. The ILC affects the lobules, i.e., the milk-producing glands. It is generally recognized that these tumors have an increased metabolic rate and an increased blood supply, which leads to a temperature spike on the breast surface that can be observed using IR thermography. Additionally, as revealed by Yahara et al. [19], the high density of blood vessels in breast cancer may play a role in the tumor and surrounding tissue temperatures.

To detect less pronounced surface temperature variations due to deeper tumors, a cold stimulation is often applied. The underlying principle is that when applying cold stress to a healthy breast, the peripheral blood flow is redirected through deeper veins, leading to a decrease in surface temperature [20]. On the contrary, an abnormal breast does not exhibit this vasoconstriction, as blood vessels produced by cancer are devoid of a muscular layer and cannot constrict in response to a cold stimulus [5]. Consequently, the affected regions appear hyperthermic in an IR image. Moreover, vasodilatation in the same regions was also observed; indeed, it was found that tumors under thermal stress produce a chemical mediator able to dilate subcutaneous vessels [14], thus increasing the surface temperature of the affected region.

Thermal images of cancerous breasts may reveal highly asymmetric temperature distributions between the left and right breasts (in the assumption that one of them is healthy), localized hot spots, and changes in hypothermic vascular patterns or variation in heat patterns in the areolar and periareolar regions [14]. In detail, according to the Ville Marie Infrared Grading Scale, a breast thermogram should be considered abnormal when at least one of the following abnormal signs is present [21]: a significant vascular asymmetry, unusual heat patterns, a temperature difference of 1 or 2 °C between the area of clinical interest and the contralateral site, a 3 °C temperature difference between the area of clinical interest and the ipsilateral breast, and a global temperature difference of 1.5 °C between the cancerous and the healthy breast.

Recently, in an attempt to isolate the blood vessels from breast thermograms to detect deeper, static heat sources (lesions), Gershenson and Gershenson [22] recognized the thermal images of the vasoconstriction of the veins due to the application of a cold stimulus. They applied the virtual wave transform technique, which is usually used in the thermal non-destructive testing field. These authors, although working with limited data, reported that the magnitude of vasoconstriction seems to be related to the presence of cancer. Due to the limitation of their data, the authors promoted future studies involving diagnostic and clinical data to validate this new paradigm.

3. Thermographic Techniques for Skin Cancer Diagnosis

Steady-state and dynamic infrared thermography were both suggested for detecting skin cancers. The steady-state thermography requires that the subject reach a sufficient thermal equilibrium with the ambient air contained in the examination room, which should be maintained at a constant temperature during the test. Dynamic thermography usually involves applying thermal stress to the skin region under investigation before acquiring thermal images. Cold stress is often used rather than a hot stimulus. One of the reasons, according to Buzug et al. [23], is that a hot stress can lead to the denaturing process of proteins when skin temperature exceeds 42 °C.

In 2014, Solivetti et al. [24] applied and compared three different techniques (high-frequency ultrasound, positron emission tomography/computed tomography, and infrared thermography) to examine 15 patients affected by advanced-stage melanoma who presented a total of 52 lesions. The results showed that the ultrasound technique was able to detect all the lesions, while tomography and IR thermography were only able to detect 24 and 15 lesions, respectively. In particular, the thermographic technique results varied according to the lesion size, and they were better for lesions greater than 7 mm. According to these authors, the ultrasound technique integrated with an accurate clinical examination could not be replaced by the other two techniques. However, no thermogram post-processing method was mentioned in their work. The lack of these post-processing techniques, along with the sole visual evaluation of the thermograms, could be the cause of the poor results obtained with IR imaging.

The possibility of distinguishing between melanomas and melanocytic nevi in both steady-state and dynamic conditions was demonstrated by Magalhaes et al. [25] using different machine learning classifiers to separately test the collected thermal images. Thermal acquisitions were performed in a room at 21 °C ± 1 °C and relative humidity less than or

equal to 50% using an FLIR E60sc IR camera with a 320×240 focal plane array, a noise equivalent temperature difference less than 50 mK at 30 °C, and a measurement uncertainty of $\pm 2\%$. Also, the quality of the recorded images was ensured by calibrating the camera with a black body source. A period of acclimatization of 10 min was considered satisfactory to reach a good thermal equilibrium to perform the IR imaging in steady-state conditions. In dynamic conditions, a 5 mm diameter aluminum disk with a thickness of 20 mm put in contact for 1 min with the skin lesion was used as a cold stimulus. In the steady-state mode, only one infrared image was acquired, while in the dynamic mode, an image was recorded immediately after the removal of the cold stimulus and the other five at each following minute. Distinctive thermal parameters to characterize the skin lesion were retrieved from the recorded images in both static and dynamic modes.

3.1. Steady-State Thermography

The examination of eleven subjects affected by BCC through steady-state thermography was reported by Flores-Sahagun et al. [26]. The infrared images were recorded using an SAT-S160 infrared camera with a low optical resolution (160×120 pixels), a temperature accuracy of $\pm 2\%$, and a temperature resolution of 0.1 °C. The camera was placed 1 m away from the patient's skin. However, no information about the acclimatization time was reported in [26]. Dimensionless temperature gradients, defined as [27], were measured between two symmetric regions of the patient's body (see Figure 1) in order to compensate the temperature readings with respect to variations in both the metabolism and ambient temperature. The authors concluded that their methodology was capable of detecting BCC in all examined cases, despite the low resolution of the instrumentation used.

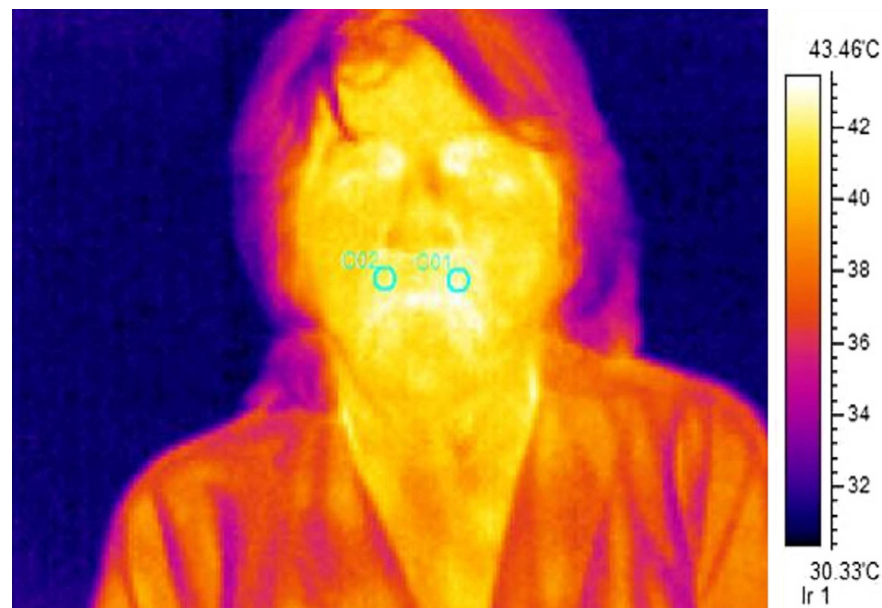


Figure 1. Infrared image of a patient exhibiting a lesion on his face, from Ref. [26]. Note that two symmetric regions were marked with blue circles. (permission asked and obtained from Elsevier, Amsterdam, The Netherlands).

A clinical study aimed at establishing the feasibility of distinguishing between benign and malignant lesions using IR thermography was reported by Shada et al. [28] in which 74 patients above the age of 18 were involved. The lesion diameter was used to classify 251 lesions, previously identified using different diagnostic tools, such as clinical diagnosis and tissue biopsy. The sensitivity (percentage of detected true positive) and specificity (percentage of detected true negative) of infrared imaging were computed for each class of diameters. Lesions of a diameter greater than or equal to 1.5 cm yielded the highest sensitivity, while smaller lesions had the lowest sensitivity [28]. Shada et al. also reported

high specificity values for all lesion sizes. However, no information about the image acquisition procedure was described in this work.

In 2015, Vardasca et al. [29] showed the feasibility of identifying malignant skin lesions through steady-state thermography by observing the thermal images of 58 patients affected by neoplasms (see Figure 2). The subjects were left to reach a sufficient thermal equilibrium with the air contained in an acclimatized room at 21 °C and a relative humidity less than 50% for 15 min before the thermal acquisition. An FLIR A325sc camera having a resolution of 320 × 240 and a precision of 70 mK, placed 80 cm away from the patient, was used to record the thermal images. The authors were able to distinguish benign from malignant skin cancers by computing the thermal contrast between two rectangular regions of interest over the neoplasm region.

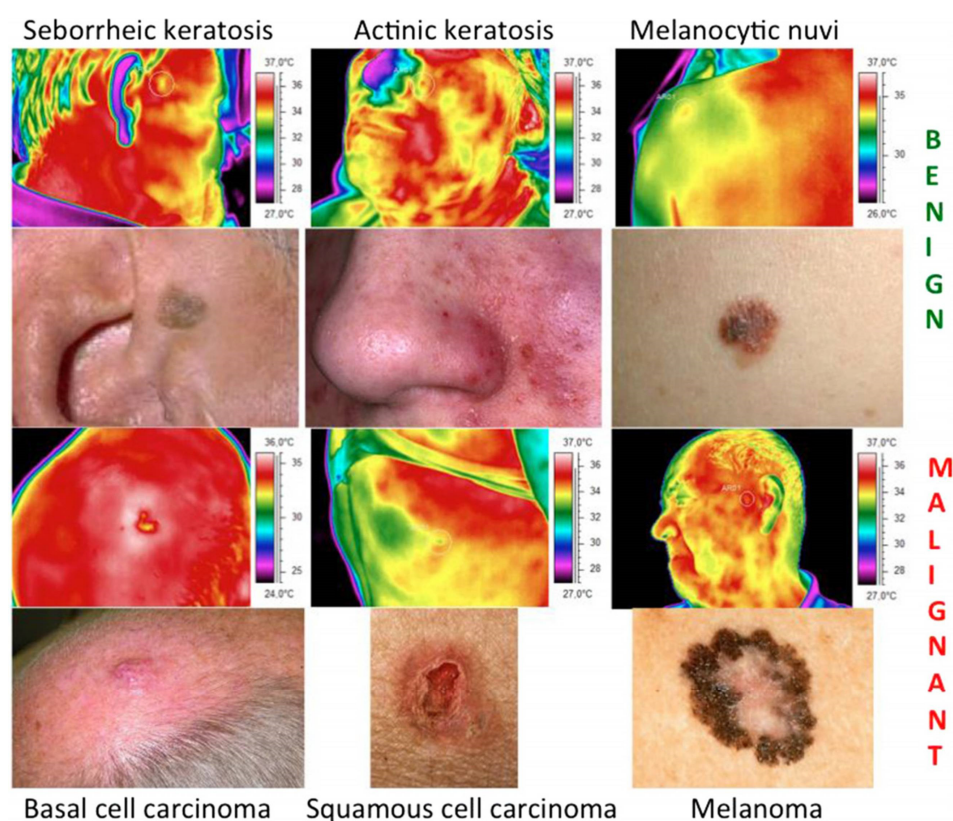


Figure 2. Example of visual and IR images of different kinds of benign and malignant skin lesions, from Ref. [29] (permission asked and obtained from IOP Publishing, Bristol, England).

To discriminate between benign and malignant skin lesions, Stringasci et al. [30] registered and analyzed steady-state thermal images of clinically similar lesions. The authors compared 100 IR images of BCC with 100 intradermal nevus, 35 images of SCC with 35 actinic keratosis, and 20 melanomas with 20 pigmented seborrheic keratosis. The infrared images were recorded through a FlukeVR FLK-Ti400 IR camera with a resolution of 320 × 240 pixels, a thermal sensitivity of less than 0.05 °C, and precision of ± 2 °C. The IR camera was placed 15 cm away from the lesion, and thermal images were recorder after the patient was hosted for 10 min in an examination room at temperature of 22 °C. Each thermal frame was analyzed in a MATLAB® environment to compute several metrics to be used within a support vector machine classifier to discriminate the lesions. Thermal images showed that actinic keratoses and SCC exhibit clearly distinct average temperatures, while the other pairs of lesions show similar temperatures. However, these similar lesions were successfully discriminated against by the support vector machine classifier using their thermal images. The authors concluded that thermography can become a diagnostic tool for the faster screening of suspicious lesions.

3.2. Dynamic Infrared Thermography

As mentioned previously, dynamic IR thermography involves a cold stimulus to enhance the thermal contrast between healthy and unhealthy skin tissues. However, in the last few years, several authors have suggested other dynamic, well-known techniques in the field of non-destructive testing, such as lock-in thermography and thermal wave imaging. Compared to classical dynamic thermography, these techniques applied for skin cancer diagnosis promise to precisely localize the lesion margins or identify the different development stages of the tumor.

3.2.1. Cold Stimuli for IR Imaging

Different skin cooling methods were investigated and compared in the scientific literature. The results obtained provide useful information when selecting a suitable cold stimulus in terms of the effectiveness of the cooling and the characteristics of the lesion.

Zenzie et al. [31] compared the skin cooling achieved through the spray and contact methods, both theoretically and experimentally, using an *in vitro* model. They concluded that both methods provide efficient skin cooling and that target depth, cost, and safety should be the deciding factors when choosing the cooling method.

Deng and Liu [32] showed that the thermal contrast between skin lesions and healthy skin can be enhanced by inducing the evaporation of water and 75% medical ethanol sprayed on the skin surface. The authors performed both numerical calculations and infrared imaging experiments on a human forearm. They found that the vascular pattern of the forearm became clearly visible several minutes after the induced evaporation. Therefore, according to the author's point of view, induced evaporation is an effective method for enhancing the skin's thermal contrast.

For three different skin cooling methods, Cheng and Herman [33] performed a computational analysis to properly select the cooling temperature, time, and cooling depth in order to maximize the thermal contrast between a lesion and healthy skin when using dynamic infrared imaging. These authors investigated idealized contact cooling at constant temperature, a water-soaked cotton patch, and convective cooling through a cold air flow or immersion into a liquid. They found that, for the three methods, the cooling effect takes less than 30 s to reach a depth of 4 mm. Also, when a cooling temperature of about 20 °C is applied, effective skin cooling is achieved; in particular, the cooling effect can reach the lesion depth within 2 min without causing discomfort to the patient. Moreover, Cheng and Herman considered cooling durations varying from 5 to 120 s; as a consequence, they studied two thermal recovery behaviors: one for short cooling times (less than 30 s) and another for longer cooling times. In particular, shorter cooling times lead to a cooling penetration depth less than 4 mm, with a maximum thermal contrast appearing within the first few seconds of the thermal recovery phase; while longer cooling durations give a lower maximum appearing 20–45 s after the removal of cold stimulus. The authors concluded that the cooling duration could be further adjusted by considering the characteristics of the lesion.

To induce deeper cooling penetration and, therefore, better thermal contrast when using dynamic IR thermography, a constant-temperature active cooling device was numerically investigated by Gomboc et al. [34]. This set-up involves a metal disk put in direct contact with the lesion and the surrounding tissue; also, a thermoelectric device (Peltier cell) mounted over the disk top provides the cooling effect. The aim was to ensure that the disk temperature was constant as possible during the cooling phase. The authors concluded that to realize faster regulation and more constant cooling temperature, the use of a thin metal disc is preferable to a thick disk. According to the authors, the set-up may be used in any tumor stage as the lesion dimensions do not affect the cooling temperature.

Recently, Verstockt et al. [35] compared different cooling techniques useful in skin cancer diagnosis when using dynamic IR thermography: conductive cooling (aluminum medal, gel pack, and ice), evaporating cooling (alcohol spray), and convective cooling (Vortex tube and Zimmer Crio 6). Skin-mimicking agar phantoms with similar thermal

properties to human skin and resembling both flat skin and an ulcerating skin lesion were used for the experimental tests. The skin phantoms were cooled for a period of 60 s, and the successive reheating process was recorded by an IR camera and two embedded resistance temperature detectors to assess the cooling penetration over time. To compare the cooling techniques, the authors defined a decision matrix considering different criteria, such as uniform cooling, repeatability, obstructing the view, cooling efficiency, workload per patient, patient comfort, use in a clinical setting, noise exposure, consumables, additional equipment, and price. The most suitable cooling method for skin cancer diagnosis was the technique that reached the highest weighted score. The authors concluded that convective cooling techniques create a more uniform cooling effect than conductive techniques, which are effective only for cooling flat objects; indeed, when they are applied to bulging skin, uniform cooling is more challenging to obtain. According to the authors, cooling methods involving ice or alcohol are unsuitable when using infrared thermography because they can compromise the accuracy of the temperature readings as they affect both the infrared radiation and the thermal camera's view. Based on their decision matrix, Verstockt et al. stated that the Zimmer Cryo 6 cooler is the best cooling method thanks to its ability to uniformly cool the skin, the consistent conditioning of cold air, high cooling efficiency at the airflow temperature of $-30\text{ }^{\circ}\text{C}$, and unnecessary consumables; on the other hand, the disadvantage of this cooling device is its cost.

Cryogenic cooling of the skin was also applied in the thermographic study, aided by numerical simulations and recently published by Verstockt et al. [36]. The authors showed that the choice of an appropriate cooling method, a cooling sequence, and an optimized experimental set-up leads to an improvement in thermal contrast.

3.2.2. Dynamic IR Thermography Using a Cold Provocation

Dynamic IR thermography was successfully applied by Buzug et al. [23] to detect a BCC. In particular, a cool gel pack was used to cool down to $27\text{ }^{\circ}\text{C}$ on a skin area of $10 \times 10\text{ cm}^2$. The thermal recovery was then recorded by an FLIR SC 3000 camera with a temperature resolution of 0.03 K for 5 min with a frame rate of 1 Hz. The involuntary movements of the patients were compensated by detecting the bore holes of a fiducial marker in the frame sequence using the generalized Hough transformation. In 2006, the work of Buzug et al. revealed dynamic thermography as a powerful diagnostic tool.

In 2009, Santa Cruz et al. began an experimental program aimed at investigating the feasibility of dynamic infrared thermography for follow-up melanoma patients treated with Boron Neutron Capture Therapy (BNCT) [37]. The patients remained at rest for 15–20 min in order to allow the examined region to reach an approximate thermal equilibrium with the environment. Then, the initial temperature distribution was recorded for 30 s (basal study); after that, an immersion in water at $15\text{ }^{\circ}\text{C}$ for 2 min or an alcohol spray followed by fan currents over the region (to induce cooling by forced evaporation) were used as cold stimuli. Again, a second thermal acquisition was recorded for 3 min or more. In order to compare the steady and post-stimulus temperature distributions, the examined region was immobilized, and anatomical landmarks were used for image acquisition. In the early phase of this study, two patients were followed up for 30 weeks after the BNCT treatment, revealing dynamic thermography as a useful tool for melanoma monitoring during BNCT treatments as well as for optimizing the treatment itself.

Cetingul and Herman developed a thermal infrared imaging system aimed at early diagnosing malignant pigmented skin lesions [38]. This system allows for small temperature differences on the skin surface to be accurately measured. In their pilot study, 37 patients with a pigmented lesion with a clinical indication for biopsy were tested. A 50 mm diameter skin region containing the lesion was cooled by a stream of cold air at $15\text{ }^{\circ}\text{C}$ for 1 min. The thermal recovery phase was recorded for 3–4 min by an infrared camera (equipped with a 320×256 pixel InSb focal plane array and having a sensitivity of $0.025\text{ }^{\circ}\text{C}$) located 30 cm away from the patient. The acquisition frequency was set at 2 s. To analyze the infrared images, an involuntary movement correction and an interactive lesion segmentation were

applied. In particular, to align the recorded thermal image sequence, the corners of an adhesive marker were used as landmarks in a quadratic motion model. Then, an interactive image segmentation algorithm was used to create a mask image delineating the lesion, which in turn was used to identify the lesion region in each of the thermal images. Cetingul and Herman reported the detection of two melanoma cases at a very early stage, for which temperature differences of 0.5 °C and 2.2 °C, respectively, between the lesion and healthy tissue were observed.

Thirty-six chronic sun-exposed subjects affected by 87 actinic keratosis and 48 BCC lesions were examined by Di Carlo et al. [39] using both dynamic IR thermography and dermoscopy. A cold stress at 5 °C on the skin area containing the lesion was applied for 20 s, and after that, the thermal recovery of this region was recorded by an FLIR3000 Thermocam. The thermal images showed well-distinct thermal patterns for the two kinds of lesions: all the actinic keratosis lesions exhibited a hyperthermic pattern, while the BCC lesions showed a hypothermic one. On the contrary, dermoscopic examination a 22% of cases for which no diagnostic indications were achievable. However, the authors stated that to confirm IR thermography as a diagnostic tool, a larger sample of subjects has to be enrolled.

Baek et al. [40] distinguished pigmented BCC and seborrheic keratosis by comparing the thermal recovery patterns of skin lesions and healthy skin recorded after the application of both hot and cold stress supplied with a thermoelectric device. Thermal images were recorded from a group of 37 patients affected by pigmented BCC (22 individuals) and seborrheic keratosis (15 individuals) and enrolled to undergo an original IR imaging procedure. After 5–10 min of acclimatization in a controlled temperature room at 23 °C and 50 ± 5% relative humidity, the skin lesion was initially heated up to 40 °C; after that, the hot stimulus was immediately removed and the thermal response of the lesion was recorded for five minutes through an FLIRVR A615 IR camera (with an optical resolution of 640 × 480 pixels and a noise equivalent temperature difference less than 0.05 °C at 30 °C). After 5 min of rest, the same lesion was cooled to 15 °C, and thermal images were acquired for the other five minutes after removing the cold stimulus. The same procedure was also applied to the healthy skin. The classification method was based on the fact that pigmented BCC showed faster thermal recovery than normal skin, whereas no significant differences between seborrheic keratosis lesions and healthy skin appeared when comparing their thermal responses.

In 2015, Godoy et al. suggested an analysis method for skin cancer screening using dynamic infrared thermography [41]. About one hundred subjects underwent the suggested method. A cold air flow produced by a Ranque–Hilsch vortex tube was used to cool the subject's skin around the suspected lesion for 30 s. Moreover, the examination room was controlled to be between 20 and 22 °C. Thermal images were acquired for a total of 2 min during both the cooling and the thermal recovery phases using a long-wave infrared camera with a 320 × 256 focal-plane array. A squared infrared marker was used to correct the involuntary movement of the subject using the Harris corner detector algorithm, and an affine transformation matrix was used to map the movements between consecutive frames. The effect of the non-uniform cooling was also considered by judiciously selecting pixels with the same initial temperature. The authors reported that their method allows 95% of the malignant cases to be correctly classified, while more than 83% of the benign lesions would be identified without the need for a biopsy.

A group of 30 patients affected by actinic keratosis were periodically monitored after the surgical removal of the lesions by Laino et al. [42], using dynamic IR thermography to evaluate the effectiveness of treatment with Eryfotona[®] in reducing the hyperthermic halo typical of this lesion. The authors employed an FLIR3000 IR camera together with patented equipment to provide the thermal stimulus. In particular, it consisted of an insulated tank containing a mixture of alcohol and water and connected, with a two-way tube, to a rubber balloon, which was put in contact with the skin. The temperature of the mixture can be set from 0 °C to 40 °C by means of a heating–cooling system embedded within the tank

walls. In their study, the patient's skin was cooled for 20 s until it reached a temperature of 5 °C. The area of the hyperthermic region and the thermal recovery time, i.e., the time the skin takes to come back to steady-state conditions, were the parameters monitored by the authors.

Dynamic IR thermography was also applied to monitor six patients affected by BCC who underwent photodynamic therapy (PDT) [43]. However, in this study carried out by Cholewka et al., a cold stimulus was not applied; on the contrary, during the photodynamic treatment, the patient's skin was illuminated by a diode laser source. Thermal images were recorded using an FLIR Thermovision Camera E60 (sensitivity of 50 mK), placed 0.5 m away from the skin lesion, before and immediately after illumination, as well as after 15, 30, and 45 min. Tests were performed in a special room whose temperature was maintained at 23 ± 1 °C. According to the authors, knowledge of the observable changes in the temperature gradient of the lesion due to the photodynamic treatment can provide useful information about chemical and physiological processes occurring during therapy.

3.2.3. Lock-in Thermography

Lock-in thermal imaging (LIT), first developed in the 1990s for non-destructive testing of materials, was first used for dermatological applications by Bonmarine and Le Gal [44]. The experimental set-up suggested by the authors foresees the use of a temperature-modulated airflow to periodically stimulate the skin surface (see Figure 3). This set-up consists of a cold air device in series with a resistive wire (whose voltage is periodically modulated) to create a temperature-modulated air flow. Moreover, thermal images were recorded by an infrared camera synchronized with the air flow modulation.

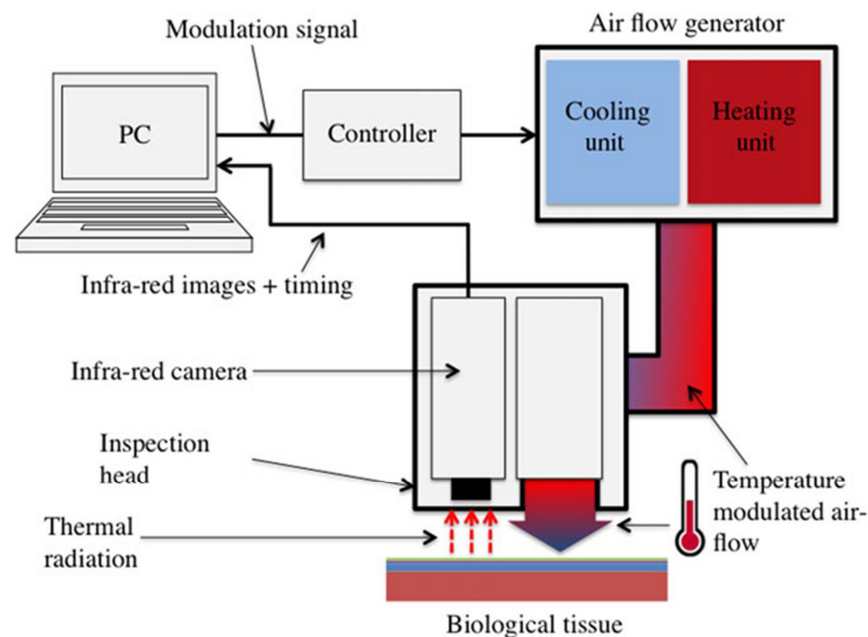


Figure 3. Schematic of the experimental set-up used for lock-in thermal imaging [44] (permission asked and obtained from John Wiley and Sons Ltd., Hoboken, NJ, USA).

Then, the acquired thermal frames had to be demodulated according to the digital lock-in principle. Applying this procedure yields a phase and an amplitude image; the former is a map of the phase angles between the thermal stimulus and the temperature response of the skin, while the second image is related to the dissipated power at the skin surface. The main advantage of LIT compared to steady-state and dynamic IR thermography is its ability to detect very small temperature gradients even when a noisy background occurs. In fact, this method is able to reject irrelevant thermal signals coming from the metabolic and circulatory variations occurring in the subcutaneous tissues [44]. Also, the suppression of the lateral heat spreading achievable in the phase image allows the lesion and its margins

to be localized accurately. Note that the same accuracy is not achievable using steady-state thermography. However, the results of the application of this method were reported by the authors only for benign skin lesions.

3.2.4. Thermal Wave Imaging

The feasibility of the frequency-modulated thermal wave imaging (FMTWI) technique used for the detection and distinction of skin cancer stages was theoretically proved for the first time by Bhowmik et al. [45] in 2005. The FMTWI technique foresees a controlled heating of the skin surface through a frequency-modulated heat flux of the desired magnitude and bandwidth, as shown in Figure 4. As a consequence, a highly diffused thermal wave propagates within the tissue, leading to time-varying temperature distributions. During the active heating, the temperature of the irradiated surface was recorded by an IR camera [45]. This method can be applied to thermally probe skin lesions at different depths using a single experimental test. Additionally, it requires a low peak power of the incident heat flux, and it is faster than other imaging techniques requiring periodically amplitude-modulated thermal excitation, such as LIT. The results showed that the FMTWI technique is suitable for the detection and differentiation of melanomas with large volumes rather than melanomas at the earliest development stages (with small volumes). Finally, by extracting the phase information from the simulated thermograms, the authors reported that the phase images have the advantage of allowing different development stages of melanoma to be clearly detected, compared to raw thermograms recorded by simply applying dynamic IR thermography.

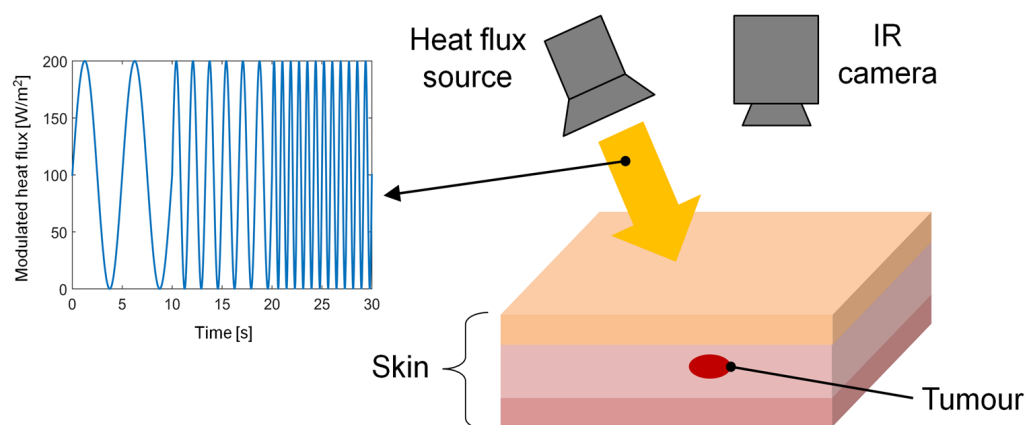


Figure 4. Schematic of the experimental apparatus of thermal wave imaging technique.

3.2.5. Literature Survey on Skin Cancer Diagnosis

The key findings and measurement protocols used in the scientific research mentioned in the above sections are summarized in Table 1.

Table 1. Summary of scientific research for skin cancer diagnosis using IR thermography.

Study	Thermal Imaging Technique	Sample Size and Lesion Type	Camera Specifications	Cooling/Heating Methods/ Acclimatization Information	Findings/Results
Gonzalez et al. [16]	Infrared Thermography.	30 patients (6 melanomas, 18 BCC, and 6 SCC).	FLIR T400 IR camera (320 × 240 FPA, spectral range 7.5–13 μm, thermal sensitivity 50 mK at 30 °C).	...	Differentiated BCC, SCC, and melanoma based on temperature differences. Correlation with vascularity.

Table 1. Cont.

Study	Thermal Imaging Technique	Sample Size and Lesion Type	Camera Specifications	Cooling/Heating Methods/ Acclimatization Information	Findings/Results
Flores -Sahagun et al. [26]	Steady-state Thermography.	11 subjects (BCC).	SAT-S160 Infrared camera (160 × 120 pixels, temp. accuracy ± 2%, temp. resolution 0.1 °C).	...	Detected BCC despite low camera resolution.
Shada et al. [28]	Steady-state Thermography.	74 patients (various lesions).	Camera specifications not provided.	...	Evaluated sensitivity and specificity based on lesion diameter.
Vardasca et al. [29]	Steady-state Thermography.	58 patients (neoplasms).	FLIR A325sc camera (320 × 240 resolution, precision 70 mK).	15 min acclimatization.	Distinguished benign from malignant skin cancers based on thermal contrast.
Stringasci et al. [30]	Steady-state Thermography.	100 cases each (various lesions).	FlukeVR FLK-Ti400 IR camera (320 × 240 pixels, thermal sensitivity < 0.05 °C, precision ± 2 °C).	10 min acclimatization.	Used SVM classifier to discriminate lesions; identified clear temperature differences for some lesions.
Buzug et al. [23]	Dynamic IR Thermography (cold).	...	FLIR SC 3000 camera (temp. resolution 0.03 K).	Cool gel pack.	Detected BCC using dynamic thermography with cold stimulus.
Santa Cruz et al. [37]	Dynamic IR Thermography (cold).	...	Camera specifications not provided.	Water immersion or alcohol spray with fan currents.	Used dynamic thermography to monitor melanoma patients during BNCT.
Cetingul and Herman [38]	Dynamic IR Thermography (Cold)	37 patients (pigmented lesions).	Unspecified IR Camera (320 × 256 pixel InSb FPA and sensitivity of 0.025 °C).	Stream of cold air at 15 °C.	Detected early-stage melanoma cases with a stream of cold air as a cooling stimulus.
Di Carlo et al. [39]	Dynamic IR Thermography (cold).	36 patients (87 actinic keratosis and 48 BCC).	FLIR3000 Thermocam.	Cold stress at 5 °C for 20 s.	Distinguished thermal patterns of actinic keratosis and BCC.
Baek et al. [40]	Dynamic IR Thermography (hot and cold).	37 patients (22 BCC and 15 seborrheic keratosis).	FLIRVR A615 IR camera (640 × 480 pixels, noise equivalent temp. difference < 0.05 °C at 30 °C).	5–10 min acclimatization, hot stress up to 40 °C, and cold stress to 15 °C after 5 min rest.	Distinguished pigmented BCC and seborrheic keratosis.
Godoy et al. [41]	Dynamic IR Thermography (cold).	About 100 subjects.	Long-wave infrared camera (320 × 256 FPA).	Cold air flow produced by Ranque–Hilsch vortex tube.	Successfully classified malignant cases using a cold air flow cooling stimulus.
Laino et al. [42]	Dynamic IR Thermography (cold).	30 patients (actinic keratosis).	FLIR3000 IR camera.	Alcohol and water mixture cooling.	Monitored effectiveness of actinic keratosis treatment with dynamic IR thermography.
Cholewka et al. [43]	Dynamic IR Thermography (laser).	6 patients (BCC).	FLIR Thermovision Camera E60 (sensitivity 50 mK).	Laser illumination (active thermography).	Investigated temperature gradient changes due to photodynamic therapy for BCC.

Table 1. Cont.

Study	Thermal Imaging Technique	Sample Size and Lesion Type	Camera Specifications	Cooling/Heating Methods/ Acclimatization Information	Findings/Results
Bonmarine and Le Gal [44]	Lock-in Thermography.	...	IR camera and temperature-modulated airflow.	Temperature-modulated air flow synchronized with the camera.	Used lock-in thermography for dermatological applications, reported results for benign skin lesions.
Bhowmik et al. [45]	Thermal Wave Imaging (FMTWI).	...	IR camera and controlled heating.	Controlled heating of the skin surface.	Theoretical feasibility of FMTWI for detection and differentiation of melanoma stages.

4. Thermographic Techniques for Breast Cancer Detection

Similarly, for a skin cancer diagnosis, steady-state and dynamic infrared thermography are both used in practice for detecting breast cancer. In fact, already at the turn of the 1990s, Ohashi and Uchida [46] tested 728 breast cancer patients using both steady-state and dynamic thermography, although the results of their study were only published in 2000. For steady-state testing, they maintained the examination room at a temperature of 21 °C in which thermal images were acquired from the front, left oblique, and right oblique directions, whereas for dynamic conditions, the subjects were exposed to cold air flow provided by an electric fan for 2 min, and after that, the thermal frames were recorded every 15 s in the anterior view. The dynamic IR images were analyzed both as sequential images and using digital subtraction, i.e., by subtracting the second of the sequentially recorded thermograms from the first one. The authors concluded that dynamic thermography reached a higher diagnostic accuracy (82%), compared to steady mode (54%).

Later in 2013, Vreugdenburg et al. [47] evaluated three different emerging methodologies suggested for breast cancer screening and diagnosis, including infrared thermography, electrical impedance scanning, and ultrasound elastography, looking for the available evidence of safety, effectiveness, and diagnostic accuracy. At that time, the authors reported that there was insufficient evidence to recommend the use of all these methodologies for breast cancer screening [47].

4.1. Steady-State Thermography

To create a data bank of normal breast thermograms, Ng et al. [48] examined 50 healthy and normal menstruating women by means of steady-state thermography to investigate the cyclic variation of temperature and vascularization of their normal breast thermograms. In fact, establishing the surface isotherm pattern of the healthy breasts and the normal range of cyclic variations of temperature over time is paramount to identifying the abnormal infrared images of diseased breasts. The examination was performed in a controlled room maintained at a temperature of 22 °C and a relative humidity between 60 and 70%. Thermal images were recorded using a contact thermogram system (encapsulated liquid crystal SINOTEST MSP8) with various thermographic plates after the subject rested for 15–20 min for acclimatization. The authors also established the best period for the thermographic examination of a female subject in relation to the menstrual cycle.

A thermographic analysis of normal breasts was also performed by Zeng et al. [49]. Their study involved 35 healthy female patients whose breasts were imaged using steady-state thermography after a break of 5–10 min for acclimatization in a room that was maintained between 21 °C and 25 °C. However, during the examination, the temperature changes were ensured to be within 1 °C. Moreover, thermal images were acquired in the anteroposterior, left and right lateral, and left and right oblique views with the IR

camera placed 1 m away from the patient. In particular, the HYIR I-1206 medical thermal imager, with an image resolution of 384×288 pixels, a temperature sensitivity of $0.08 \text{ }^\circ\text{C}$, and operating in the spectral range of $8\text{--}14 \text{ }\mu\text{m}$, was employed. The authors found evidence that the temperature distribution of healthy breasts was symmetrical and that the mean temperatures of both breasts were almost equal. However, slight differences in the temperature were reported between the upper left and right quadrants and between the upper and lower quadrants.

Wang et al. [50] selected a group of 276 women who were scheduled to undergo an excisional biopsy based on mammograms or ultrasounds to be examined using steady-state thermography the day before surgery. Each participant rested for 15 min on a chair in an erect position with their hands over the head in a controlled-temperature room maintained at $23\text{--}25 \text{ }^\circ\text{C}$. After that, two lateral and two oblique views of IR images were recorded using an ATIR-M301 thermal imaging system (with a 320×240 focal plane array detector and a temperature resolution less than $0.1 \text{ }^\circ\text{C}$) placed 2.5 m away from the subject. To investigate the diagnostic performance of the IR thermography, the authors analyzed the collected thermal images by evaluating five independent diagnostic signs by means of statistical analysis. In particular, they defined univariate and multivariate logistic regression models to investigate the correlation between IR signs and the final disease status assessed by biopsy. The authors predicted sensitivity and specificity values of 72.4% and 76.6%, respectively.

Low sensitivity values for digital infrared thermal imaging applied under steady-state conditions were reported by Kontos et al. [51] in 2011. These authors examined 63 patients using the Meditherm med2000 thermal imaging system. A series of the recorded thermal images is shown in Figure 5. The examination was performed in a room without windows, in which the temperature was approximately maintained at $22 \text{ }^\circ\text{C}$. Also, the patients were left to acclimatize with ambient air for 10–15 min before sitting on a rotation stool (without a back rest) placed 1 m away from the thermographic camera. The authors concluded that steady-state infrared imaging should not be used as a screening test for breast cancer detection, and it was also not suitable for the primary evaluation of symptomatic patients because of its low sensitivity.

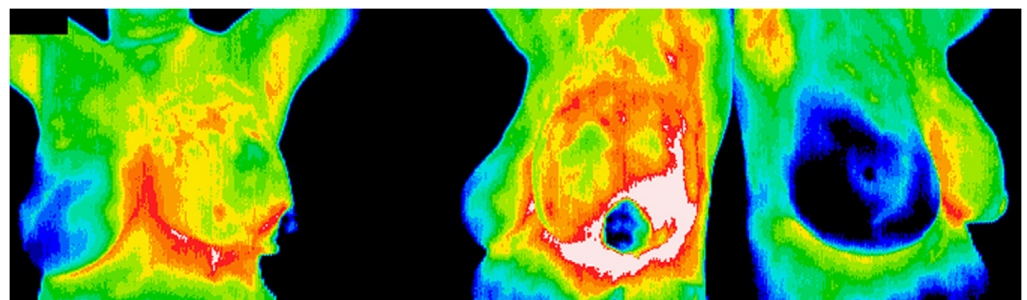


Figure 5. Thermal images of a patient having a suspicious lesion on the left breast, from Ref. [51] (permission asked and obtained from Elsevier, Amsterdam, The Netherlands).

Morais et al. [52] examined a group of 47 breast cancer patients using the same dimensionless temperature gradient-based methodology described in [26]. In their study, the following two different IR cameras were employed: a ThermoCAM T400 FLIR E60 (with a resolution of 320×240 pixels and a temperature sensitivity of $0.05 \text{ }^\circ\text{C}$) and an SAT-S160 camera with a low optical resolution (160×120 pixels) and lower temperature sensitivity ($0.1 \text{ }^\circ\text{C}$). Figure 6 shows a thermal image recorded by the highest performance camera. The authors reported that their methodology was efficient in identifying breast lesions even when a lower-resolution camera was used. Therefore, they concluded that their methodology can be potentially used as a non-invasive screening tool.

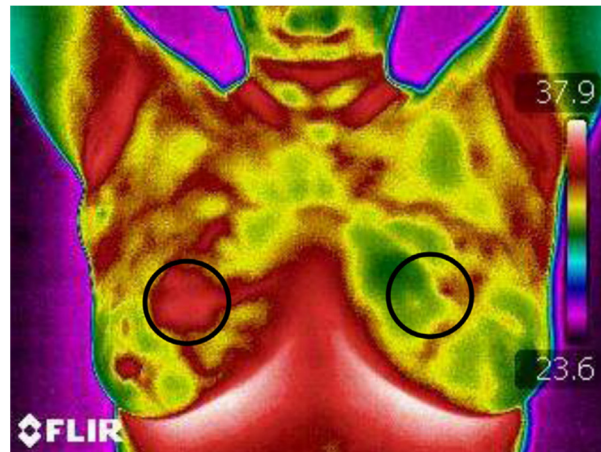


Figure 6. Breast infrared image of a patient with a high asymmetry, as highlighted by the circles drawn in the figure, from Ref. [52]. (permission asked and obtained from Elsevier, Amsterdam, The Netherlands).

4.2. Dynamic Infrared Thermography

To enhance the thermal contrast due to smaller and deeper breast tumors, dynamic imaging after or during the application of a cold stimulus was performed. In addition to canonical dynamic breast thermography, an alternative procedure known as rotational thermography was suggested to allow the whole breast surface to be imaged.

4.2.1. Cold Stimulus and Patient Comfort

Contrarily to steady-state thermography, patient comfort related to the application of cold stress is a crucial aspect of dynamic breast IR imaging. Indeed, to improve the thermal contrast between the cancerous and healthy breast, a cold air flow typically between 5 °C and 15 °C is often blown to the patient's breast while holding their hands on the head [13]. Also, the cooling period ranges between 2 min and 6 min to create a sufficient thermal contrast to detect tumors at depths less than 15 mm. Obviously, a longer cooling period yields a higher thermal contrast but more discomfort for the patient. Contact cooling methods are also applied in fewer cases.

According to the numerical results provided by Amri et al. [53] to ensure both a good thermal contrast and better patient comfort, cold air flow at temperatures just below the ambient temperature can be applied for less than 1 min.

A numerical study to optimize the cooling stress applied for early detection of breast cancer from dynamic IR images was performed by Zhou and Herman [54]. Thermal contrasts observable when applying a cold stress for a duration of 15–25 min at a constant cooling temperature of 5–15 °C on the skin surface were analyzed using a 2D breast model by simulating tumors of different sizes, depths, and locations. The authors reported that to achieve the maximum thermal contrast for deeper and smaller tumors, the tissue should be cooled for 5–15 min; also, this maximum appears after 20–45 min during the thermal recovery phase [54]. Notwithstanding, the thermal signature of smaller tumors close to the muscle layer can be covered by the underlying layers at core body temperature, limiting the ability to detect lesions.

The efficacy of dynamic cooling was tested by Sadeghi et al. [55] using a gel phantom mimicking the human breast affected by a tumor. A depth-adjustable heat source (a resistor having dimensions of 2 mm × 1 mm) simulating a tumor was placed inside the gel phantom, in which three temperature sensors were also embedded. The temperature of the phantom was maintained at 37 °C through a heating plate placed underneath, whereas the simulated tumor was kept at 39 °C. A cold stimulus was simulated using a glass container filled with water at 18 °C. After its removal, the thermal recovery of the phantom was recorded by an FLIR A65 IR camera. The authors found that although the tumor depth affected

the temperature spread on the phantom surface, the mimicked tumor was detectable at different depths. Additionally, they reported that a cooling time of 3 s was sufficient to induce cold stress on the phantom.

4.2.2. Dynamic IR Thermography Using a Cold Provocation

The effectiveness of dynamic IR thermography in distinguishing between benign and malignant breast lesions was assessed by Parisky et al. [56]. Thermal images of 769 subjects with 187 malignant and 688 benign lesions, previously evaluated through mammography, were acquired in a rapid sequence both before and during the cooling phase. In particular, in this phase, a stream of cold air supplied by a refrigeration chamber was circulated around the breast. The authors reported high sensitivity values (97%) and poor specificity (14%), which, however, was statistically higher in dense breast compared to fatty breast. The authors recognized the value of dynamic IR imaging in conjunction with mammography in determining whether a lesion is benign or malignant.

The effectiveness of a dynamic IR breast scan, known as Sentinel BreastScan™, was evaluated in 2008 by Arora et al. [57], testing 92 women with suspicious breast lesions. The IR system was equipped with an IR camera with a 320×240 uncooled focal plane array, a sensitivity of $0.08 \text{ }^\circ\text{C}$, and an operating wavelength range of $7\text{--}12 \text{ }\mu\text{m}$. The examination was performed in dynamic conditions using an air cooler supplying a cold air flow directed toward the breasts and a chair equipped with lateral-view side mirrors. More than 100 thermal images were gathered for approximately 4 min for each patient. The authors applied three different modes for analyzing thermal frames, and in particular, a screening mode, a clinical mode based on prior information related to the lesion location, and an artificial neural network. They reported sensitivity values higher than or equal to 90% for each mode, and they concluded that digital IR thermography is a valuable adjunct to mammography and ultrasound, especially in all those cases in which the diagnosis of breast cancer can be difficult (such as in younger women, men, patients with dense breasts, or patients with surgically altered breasts).

The accuracy of the same IR breast scan employed in the study of Arora et al. was assessed later in 2010 by Wishart et al. [58]. These authors subjected 100 women with suspicious breast lesions to IR imaging before their biopsy. For each patient, a sequence of 250 thermal frames was acquired while they were sat on an ergonomic chair with their arms supported at eye level, and a temperature-controlled air flow was directed at the breasts for about 5 min. The recorded images were analyzed using proprietary software. The authors concluded that digital infrared imaging is particularly effective for breast cancer detection in women under 50 years old, for which they observed the maximum values of sensitivity (78%) and specificity (75%).

Sarigoz and Ertan [59] evaluated twenty-six patients affected by IDC of the breast through dynamic infrared thermography before surgery. The examination room was kept at a constant $22\text{--}25 \text{ }^\circ\text{C}$ with a relative humidity of around 50%. After 15 min for acclimatization, two initial steady-state images of the axillary region were recorded using a Fluke® Ti9 IR camera (with an image resolution of 640×480 pixels and thermal sensitivity $\leq 0.20 \text{ }^\circ\text{C}$ at $30 \text{ }^\circ\text{C}$) placed at a distance of 1 m. Then, a cold stress was applied to the same region using a gel pack at $4\text{--}8 \text{ }^\circ\text{C}$ for 2 min. The successive thermal recovery was recorded for at least 2 min, and sequential thermal frames were taken every 5 s. The authors reported an achieved sensitivity of 83% and a false negative rate of 16% when diagnosing axillary involvement. Finally, dynamic infrared thermography was found to be superior to ultrasound, mammography, and magnetic resonance imaging in detecting malignant lymph nodes.

4.2.3. Rotational Breast Thermography

Very often in conventional breast thermography, the patient placed in front of the camera is imaged in three different views, namely contra-lateral, medio-lateral oblique, and axillary. However, in these views, the lower posterior regions of the breast are not

imaged completely because of the normal breast sag [20]. Consequently, cancerous lesions in such regions are not detectable. To overcome this limitation, a novel technique, known as rotational breast thermography, was suggested. This technique foresees that the patient is lied in prone position on a special set up known as the Mammary Rotational Infrared Thermographic System (MAMRIT), with one breast freely suspended into a temperature-controlled closed chamber through a small circular aperture. Also inside this chamber is a robotic arm, within which an infrared camera is fixed, that rotates clockwise around the suspended breast so that it can be imaged from many perspectives. In such a way, the whole breast surface can be completely analyzed, ensuring that all abnormalities are detected.

The potential of rotational thermography for the automatic detection of breast abnormalities involving a cold stimulus was evaluated by Francis et al. [20]. In particular, these authors assessed the accuracy of this technique both before and after the application of a cold stress that was performed by cooling the temperature of the closed chamber by 2–3 °C. A group of 36 patients (24 healthy and 12 with breast abnormalities) were involved in this study. Also, steady-state thermograms were recorded after a period of rest to stabilize basal metabolic activity, with the air temperature inside the chamber adjusted to the comfort level of the patient and a relative humidity of 60%. In both steady and dynamic conditions, a series of 12 images were acquired for each breast at spatial intervals of 30°. After that, statistical and texture features were extracted from the rotational thermogram series in both conditions. Then, these features were used as inputs within a support vector machine able to automatically classify healthy and malignant breasts. The authors reported better accuracy in steady conditions (about 83%) when compared to that obtained (about 70%) from the thermograms recorded after the cold stimulus. In conclusion, the authors stated that rotational thermography holds great potential as a screening tool for breast cancer detection, especially when it is used as an adjunct tool to ultrasound.

4.2.4. Literature Survey on Breast Cancer Diagnosis

The scientific research mentioned in Section 4 is summarized in Table 2.

Table 2. Summary of scientific researches for breast cancer diagnosis using IR thermography.

Study	Thermal Imaging Technique	Sample Size and Lesion Type	Camera Specifications	Cooling/Heating Methods/ Acclimatization Information	Findings/Results
Head et al. [17]	Infrared Thermography.	326 patients.	Camera specifications not provided.	...	Demonstrated increased risk of breast cancer in subjects with abnormal IR breast images.
Ohashi and Uchida [46]	Infrared Thermography.	728 breast cancer patients.	Camera specifications not provided.	Cold air flow provided by a fan for 2 min.	Reached diagnostic accuracy of 82% in dynamic conditions.
Ng et al. [48]	Steady-state Thermography.	50 healthy women.	Encapsulated liquid crystal SINOTEST MSP8.	15–20 min acclimatization.	Investigated cyclic variation of temperature of normal breast thermograms.
Zeng et al. [49]	Steady-state Thermography.	35 healthy women.	HYIR I-1206 (384 × 288 resolution, sensitivity of 0.08 °C).	5–10 min acclimatization.	Demonstrated thermal symmetry in healthy breast.
Wang et al. [50]	Steady-state Thermography.	276 women with previous diagnoses.	ATIR-M301 camera (320 × 240 FPA, temp. resolution < 0.1 °C).	15 min acclimatization.	Investigated correlation between IR signs and final disease status.

Table 2. Cont.

Study	Thermal Imaging Technique	Sample Size and Lesion Type	Camera Specifications	Cooling/Heating Methods/ Acclimatization Information	Findings/Results
Kontos et al. [51]	Steady-state Thermography.	63 patients.	Meditherm med2000 thermal imaging system.	10–15 min acclimatization.	Steady-state infrared imaging should not be used for breast cancer screening.
Morais et al. [52]	Steady-state Thermography.	47 breast cancer patients.	ThermaCAM T400 FLIR E60 (320 × 240 resolution) SAT-S160 (160 × 120).	...	Identified breast cancer lesions using different resolution cameras
Parisky et al. [56]	Dynamic IR Thermography (cold).	769 patients (187 malignant; 688 benign lesions).	Camera specifications not provided.	Stream of cold air supplied by a refrigeration chamber.	Distinguished between benign and malignant lesions.
Arora et al. [57]	Dynamic IR Thermography (cold).	92 women (suspicious breast lesions).	Sentinel BreastScan™ (320 × 240 FPA, sensitivity of 0.08 °C).	Cold air flow supplied by an air cooler.	Obtained high sensitivity values.
Wishart et al. [58]	Dynamic IR Thermography (cold).	100 women (suspicious breast lesions).	Sentinel BreastScan™ (320 × 240 FPA, sensitivity of 0.08 °C).	Cold air flow for 5 min.	Demonstrated effectiveness of IR imaging for breast cancer detection in women under 50 years old.
Sarigoz and Ertan [59]	Dynamic IR Thermography (cold).	26 patients (IDC).	Fluke® Ti9 IR camera (640 × 480 resolution, sensitivity ≤ 0.20 °C).	Gel pack at 4–8 °C for 2 min.	Demonstrated superiority of IR imaging superior than other imaging techniques in detecting malignant lymph nodes.
Francis et al. [20]	Rotational Thermography.	36 patients (24 healthy and 12 abnormal breast IR images).	Camera specifications not provided.	Cold air in a closed chamber.	Demonstrated the potential of rotational thermography.

5. Skin Tissue Modeling

5.1. Forward Modeling

The most common modeling of the skin tissues used in the literature involves a five-layer structure consisting of the epidermis, papillary dermis, reticular dermis, fat layer, and muscle, as shown in Figure 7. One-dimensional (1D), two-dimensional (2D), or three-dimensional (3D) models based on the Pennes equation are encountered in the literature.

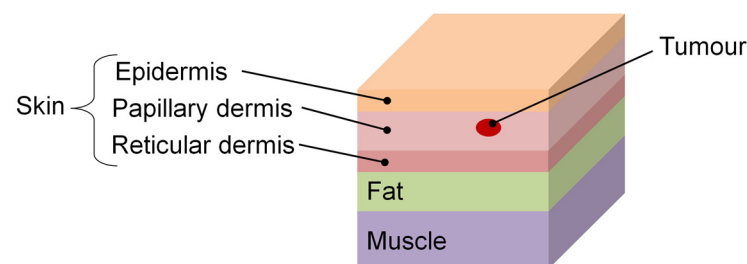


Figure 7. Schematic of a five-layer skin tissue model with an embedded tumor.

An exception is the work authored by Deng and Liu [60], who considered a simplified three-layer skin model consisting of a skin, fat, and flesh layer with cancer tissue inside. To reveal the correlation between skin surface temperature and interior human pathophysiology, these authors solved a transient 3D bio-heat transfer problem involving a

non-linear boundary condition at the skin surface (due to simultaneous heat transfer by convection, radiation, and evaporation) using the Monte Carlo method. Different factors affecting the skin temperature and consequently the temperature reading recordable with an IR camera were investigated: skin emissivity, skin humidity, convective heat transfer coefficient, temperature and relative humidity of ambient air, metabolic rate and blood perfusion in the tumor, and lesion size. The authors found that the obtainable thermal contrast is strongly correlated with the lesion size and the metabolic rate in the area affected by the lesion [60].

Irregular-shaped skin lesions were considered by Cetingul and Herman [61] in a 3D multilayer skin model similar to that depicted in Figure 7. These authors assessed the sensitivity of surface transient thermal responses with respect to the variations in thermophysical properties, metabolic heat generation, blood perfusion rate, and thicknesses of skin layers. Their model involves a constant-temperature boundary condition applied to the skin surface to simulate the cold stimulus, while convective heat transfer on the same surface describes the thermal recovery. A similar 3D model was used by the same authors in [62].

A 2D semi-infinite multilayer skin model involving an elliptical lesion located in the papillary dermis layer was studied by Cheng and Herman [33] to investigate the skin cooling effect provided by different cooling methods.

A bio-heat transfer model integrated with the momentum and energy conservation equations for non-Newtonian blood flow within multi-layer skin was suggested by Bhowmik et al. [63]. In particular, they considered a 3D multilayer model with counter-current blood vessels in each skin layer, as well as various cancerous lesions with different geometrical, thermal, and physical parameters. Following the dynamic infrared thermography procedure, the rewarming period of the skin was simulated by taking free convection, radiation, and evaporation into account. The evaluation of the skin thermal response highlighted that subsurface blood flow overpowers the response of early-stage melanomas.

In order to theoretically evaluate lock-in thermal imaging for the early detection of melanomas, Bonmarin and Le Gal [64] used a Pennes equation-based 2D axisymmetric multilayer skin model to simulate the steady state and transient surface temperatures. The skin lesion is modeled as a cylindrically shaped region with different thermophysical properties compared to the surrounding healthy tissue. Also, boundary conditions applied to the top surface take convective and radiative heat transfer between the skin and thermally modulated air flow into account. The authors concluded that melanomas can be successfully detected by applying the lock-in demodulation formalism to the transient skin surface temperature. This is also true when the lesion is at the early-stage of development, i.e., when its penetration depth is less than 0.1 mm.

Iliaz et al. [65] developed efficient solvers to compute the steady-state and transient solutions of a bio-heat transfer problem in skin tissue. In particular, the addressed problem involves a 2D multilayer skin model including a melanoma of different sizes. Also, in this work, the cooling–rewarming conditions reported in [37] were considered. The subdomain approach of boundary element method (BEM), which is faster than the classical BEM, was applied as numerical solution technique. The authors showed that the use of the BEM parabolic formulation with quadratic elements yields high accuracy and reduces computational times. For this reason, they suggest this solver for inverse bio-heat transfer problems aimed at retrieving lesion size and parameters.

Finally, an example of steady-state skin tissue modeling used to establish whether the underlying lesion is benign or malignant is discussed by Agyingi et al. [66].

5.2. Inverse Modeling

Inverse procedures that are useful for estimating thermophysical parameters and growth features of skin lesions are gaining more and more interest due to the increasing development of IR cameras and computational capacity. Indeed, information regarding the thermal properties of a lesion leads to more reliable numerical models, and on the other

hand, an accurate estimate of the lesion penetration depth provides relevant information about the tumor stage to which it is related [67], reducing the cases of unnecessary biopsies required for stage characterization.

An inverse procedure aimed at estimating the size and location of a skin lesion was applied by Partridge and Wrobel [68] using a dual reciprocity boundary element method coupled with a genetic algorithm. The temperature measurements at the skin surface were obtained from a steady-state 2D model involving a lesion located at different depths, in which both a second and a third-kind boundary condition at the skin surface were applied. The absence of internal nodes, the unnecessary computation of sensitivities, and the unnecessary definition of an initial guess location of the lesion are the main advantages of the suggested procedure [68]. However, the authors reported that very small or deeply located tumors cannot be detected using this procedure as they produce only a small perturbation of the skin temperature.

Simplified 2D and 3D skin models based on the steady-state bioheat Pennes equation were used by Agnelli et al. [69] to estimate the unknown metabolic heat generation or geometrical parameters of a circular or spherical tumor lesion included in the computational domain. A second-order finite difference scheme was applied to obtain the simulated surface temperature distributions used in the inverse procedure, which was based on the Pattern Search algorithm. The authors reported very good estimation accuracy for both 2D and 3D cases, even when the simulated data were affected by a noise level of 5–10%.

Two stochastic algorithms (such as the genetic algorithm and simulated annealing) were applied by Bhowmik and Repaka [70] for simultaneously estimating the diameter, penetration depth, blood perfusion, and metabolic heat generation of subsurface skin cancers based on the surface temperature variations obtained from a 3D model of human skin. In this work, the forward model required the numerical solution of the Pennes bioheat equation for a multilayer skin (see Figure 7) whose top surface can exchange heat with the external environment by convection, radiation, and evaporation. Also, the cooling phase was simulated by applying a first-kind boundary condition (imposed temperature) to the top surface. The simulated annealing algorithm was found to be superior with respect to the genetic algorithm. In fact, the computing time is shorter, and the retrieved parameters have a higher accuracy when using the former algorithm. The authors concluded that their algorithm, along with a thermal camera, may provide a useful diagnostic tool for the characterization of subsurface skin lesions.

Stratowsha et al. [71] estimated the perfusion coefficient, thermal conductivity, and thermal heat capacity of skin tissue using inverse thermal modeling based on the Laplace transform method and the related Nyquist's plots. The time domain thermal response was predicted by a 1D three-layer skin model using the Pennes equation, while the temperature measurements were obtained from a person's forearm by applying dynamic IR thermography. The authors reported a measurement uncertainty of less than 30% and that they were going to apply this approach for screening malignant and benign skin lesions.

Later, in 2018, the same authors applied the same procedure to classify psoriatic lesions and healthy skin regions [72]. However, a more complete thermal model involving metabolic heat generation was considered by the authors.

Iliaz et al. [73] applied the Levenberg–Marquardt algorithm for the simultaneous estimation of tumor diameter, thickness, blood perfusion rate, and thermoregulation coefficient when using dynamic infrared thermography. The authors simulated the measured skin temperature distribution by adding noise to the numerical solution of a 3D bio-heat transfer problem involving the cylindrically shaped multi-layer skin model described in [74]. In addition, the cold stimulus is simulated through a first-kind boundary condition, while the thermal recovery is described using Robin's boundary condition by neglecting radiative heat transfer as well as heat loss due to evaporation. According to the authors, an accurate estimation of lesion diameter and thermoregulation coefficient can be attained regardless of the noise and tumor stage, whereas the blood perfusion rate and lesion thickness can only be accurately estimated for a low noise level or later tumor stage.

A time-consuming inverse solution method for the bio-heat transfer problem addressed in [65] was described by Iliaz et al. [75]. They stated that the blood perfusion rate, metabolic heat generation, diameter, and thickness of the tumor can be simultaneously estimated.

Chen et al. [76] estimated the depth, sizes, and thermal properties (thermal conductivity, heat generation, and blood perfusion) of skin tumors using a deep learning model and a 3D finite element, five-layer skin model. Skin surface temperatures during the thermal recovery phase were simulated by varying the features of a rectangular tumor lesion, and the obtained temperature data were used to train and test the performance of the neural network. The authors concluded that the deep learning model can establish a relationship between the skin surface temperature and the tumor features, allowing not only to estimate its thermal properties but also to retrieve tumor heat generation and blood perfusion.

6. Mammary Tissue Modeling

Human breast geometry is commonly modeled as a hemispherical volume consisting of different concentric tissue layers, such as the core glandular, subcutaneous glandular, and fatty and skin layers. In the simplest models, all these layers have a uniform thickness in the whole domain, as shown in Figure 8a. Non-concentric multi-layer models are also possible (Figure 8b). Moreover, both 2D and 3D models based on the Pennes equation are considered in the literature.

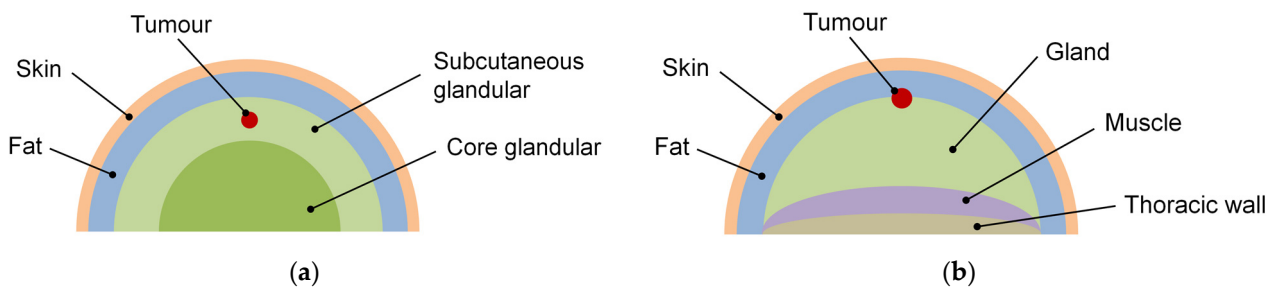


Figure 8. Cross-section of 3D breast tissue multi-layer models with an embedded tumor: (a) concentric layers; (b) non-concentric layers.

As far as 3D models are concerned, a third-kind boundary condition involving a constant heat transfer coefficient is often applied at the breast surface, while at the interface between the chest and breast, an imposed constant temperature is usually considered.

Additionally, anatomical or more realistic breast models have also been suggested by several authors in order to consider the complexity of the glandular tissue and the actual breast's geometry. Although these realistic models require greater modeling efforts than simplistic models because, in fact, they involve different technologies to reproduce the actual geometry and to exactly locate the tumor lesion, they yield more accurate and realistic results as they also benefit from the use of real clinical data.

6.1. Forward Modeling

To reveal the complex correlation between the breast thermal behavior and the underlying pathophysiological conditions, different numerical modeling techniques have been proposed. The principal ones are reviewed below.

A 3D finite element model aimed at investigating the effect of the thermal and elastic properties of breast tissues on the thermal contrast of both healthy and cancerous breasts was developed by Jiang et al. [77]. In particular, the undeformed human breast was modeled as a hemispherical volume consisting of four concentric tissue layers with a uniform thickness, as depicted in Figure 8a. Then, gravity-induced deformation was introduced by applying both linear and non-linear elastic models. Moreover, both static and dynamic thermal conditions were considered in this work. The authors found that at the steady-state, for normal body posture (sitting or standing), gravity-induced breast

deformation yields an upper-lower asymmetric surface thermal contrast. Also, the surface temperature changes due to the lesion were more sensitive to tumor depth than its size. In dynamic conditions, the results obtained suggested that the tumor-induced thermal contrast exhibits an opposite initial change and delayed peak when compared to the deformation-induced thermal contrast on the breast surface. According to the authors, these lags of the thermal contrast are generally longer in deeper tumors that also show smaller peaks.

A finite element model involving a realistic breast geometry based on 3D scanning of a mannequin was defined by Mukhmetov et al. [78] to improve the accuracy and reliability of computer-aided diagnosis. To experimentally validate their model, the authors created a silicon rubber breast using 3D printing and molding techniques. Also, the presence of a tumor lesion was simulated through resistors placed within the silicone breast. This study revealed that 3D breast geometry and tumor size can give different temperature profiles, affecting the precision of computer-aided diagnosis of breast cancer. In fact, the authors reported that the maximum temperature difference between healthy and cancerous breasts can range from 0.34 to 1.37 °C when the cup sizes range from 120 to 260 mm and a tumor depth from 5 to 25 mm.

A finite element, four-quadrant flexible breast model was developed by Ng and Sudharsan [79]. These authors imagined the human breast divided into four quadrants, namely the upper-outer quadrant, the upper-inner quadrant, the lower-inner quadrant, and the lower-outer quadrant. In such a way, the thermal properties of the tissues in each quadrant could be changed selectively, yielding flexibility in the simulation. The suggested model not only incorporates three tissue layers (subcutaneous fat, a gland layer, and a core region) with different thicknesses, but it also includes the areola region as a separate entity. Also, to define a more realistic geometry, the outer breast profile of a mannequin was traced with a CNC machine. The authors validated their model using experimental steady-state thermograms, and they reported a good overall match.

A realistic computational thermal model of the human breast calibrated to real clinical data was developed by Lozano et al. [80] using high-resolution infrared images, real 3D breast geometries, and magnetic resonance imaging. For the purposes of their study, a female subject histologically diagnosed with breast cancer was enrolled. In particular, the real breast geometry was accurately derived using a 3D scanner. Additionally, magnetic resonance images were used to create the back surface of each breast based on the anatomic curvature of the pectoral muscle and to model the skin layer thickness around the nipple region, as well as to gain insight about the location and irregular geometry of the cancerous lesion. Moreover, the thermal properties (blood perfusion and metabolic heat generation rate) of both healthy and cancerous breast tissues were obtained by choosing those that best matched the surface temperature distributions recorded by an IR camera. According to the authors, the results obtained may be applied to cases with similar breast cancer features.

Unlike the previous authors, Amri et al. [53] considered a simplified 3D breast model that consists of a two-layer finite plate representing a fat layer and the gland region. Also, a spherical-shaped lesion was placed inside the deeper layer. The bio-heat transfer problem was solved numerically by means of the transmission line matrix technique [81]. Both steady-state and dynamic conditions were simulated by the authors. They reported that steady-state thermal contrast depends both on the depth and size of the lesion. It is also affected by breast density; fatty breasts lead to lower thermal contrasts; on the contrary, dense breasts result in increased thermal contrasts. Finally, in dynamic conditions, they found that after the application of a cold stress, the consequent transient thermal contrast may potentially provide valuable information about the tumor depth when it is analyzed using signal processing techniques.

The effect of breast density on the surface temperature distribution was further investigated by Wahab et al. [82], who developed four different 3D breast models with different compositions. All the models were based on a three-layer configuration consisting of a muscle layer, a glandular layer, and a subcutaneous fat layer. In particular, the breast

geometry was represented by a hemispherical shape with non-concentric internal layers (as in Figure 8b). On the contrary, the tumor was modeled with a perfect spherical shape embedded in the breast model. The authors concluded that breast density may affect the surface temperature distribution and should be considered in breast cancer detection when using infrared thermography.

Finally, the effects of tumor depth, tumor size, metabolic heat generation rate, blood perfusion, and thermal conductivity on the breast surface temperature distribution in steady-state conditions were analyzed by Al Husaini et al. [83]. These authors employed a 3D finite element hemispherical breast model consisting of four layers (muscle, gland, fat, and skin). Different breast sizes were also considered in their work. The results obtained showed that larger breasts consistently reduce surface temperature variations, leading to some difficulties in observing significant thermal contrasts between cancerous and healthy breasts. Additionally, tumors smaller than 0.5 cm and located in smaller breasts may be difficult to detect, as they could not yield observable temperature variations. The same also occurs for tumors located deep within the breast layers.

6.2. Inverse Modeling

Inverse thermal modeling techniques can be applied to estimate the exact location and size of a breast lesion. Attempts to evaluate the blood perfusion rate of this tumor are also discussed by different authors.

The problem of the identification of both thermophysical (thermal conductivity, perfusion coefficient, and metabolic heat generation) and geometrical parameters (location and size) of a tumor lesion was investigated by Paruch and Majchrzak [84]. These authors addressed both 2D and 3D problems using an evolutionary algorithm coupled with the multiple reciprocity boundary element method. In the second and more interesting problem, the breast was modeled as one half of the ellipsoid, including a tumor lesion with a similar geometry. Real values of unknown parameters were obtained, but the algorithm implemented by the authors was time-consuming, especially in the case of a 3D problem.

Das and Mishra [85] applied the curve fitting method to simultaneously estimate the size, radial location, and angular location (described by two angular coordinates) of a tumor present in a 3D human breast. In particular, a simplified hemispherical model of the breast based on the Pennes bio-heat equation was used to compute the skin surface temperature profile. The suggested procedure did not require solving the governing equation, and the estimation was very fast. The authors reported smaller estimation errors when a tumor of larger size located close to the skin surface was considered. The same inverse procedure was previously tested by the same authors, considering a simplified 2D geometry [86].

More accurate finite element 3D breast models were investigated in the inverse analysis performed by Hossain and Mohammadi [87]. In particular, these authors suggested both an undeformed model and a dropped (ptosis) breast model; the former concerns a hemispherical model consisting of three layers (lobule, fat, and skin layers) at the base of which a muscular layer is placed, while the latter is partitioned into three parts, namely a lower hemispherical part, a cylindrical middle segment, and an upper cylindrical wedge region showing a 45° angle with the chest. In both models, a spherical cancerous lesion is submerged entirely in the lobular region. Simulated steady-state temperature distributions computed through the described models were then used in a customized genetic algorithm to retrieve metabolic heat generation and lesion location. The authors reported a very good accuracy of the estimated parameters, even when a noisy level of 10% is considered.

A surrogate 3D breast geometry was developed by Ferreira de Melo et al. [88] using the breast profile curve obtained from IR images. Moreover, an external prosthesis was used to dimension the thoracic wall in order to adjust the total volume of the model. Additionally, a cancerous lesion was accurately inserted in the model using the information provided by an ultrasound examination. Once the bio-heat transfer problem was defined, the authors applied the sequential quadratic programming method to estimate the thermal conductivities of glandular and nodule tissues. The authors claimed that their new geometry allowed

the tumor thermal conductivity to be estimated compared to that defined by other authors in a similar work [89].

A 2D hemispherical model of an axisymmetric tumorous breast was applied by Hatwar and Herman [90] in an inverse analysis to simultaneously estimate the size, location, and blood perfusion of the lesion. In particular, the considered hemispherical model involves six tissue layers (namely epidermis, papillary dermis, reticular dermis, fat, gland, and muscle layers) and a spherical tumor located at the axis of the hemisphere. It is worth noting that the thickness of the gland and the muscle layers are not uniform in the breast model (as shown in Figure 8b), whereas the others are uniform. The Pennes bio-heat equation was solved in such a domain to generate both the steady-state and transient surface temperature distributions recordable by IR imaging. In particular, the cooling phase was modeled by imposing a constant-temperature boundary condition. Then, the Levenberg–Marquardt algorithm was iteratively used to estimate the tumor features. The authors performed several numerical tests by varying the depth, radii, and blood perfusion of the tumor. They concluded that the simultaneous estimation of blood perfusion, size, and location of the tumor is possible only when transient temperature data are considered.

Figueiredo et al. [18] estimated the location of the geometric center of the three major types of mammary lesions using an anatomical 2D breast model without the need for prior knowledge of the tumor's thermophysical properties. The authors simulated the steady-state temperature distribution of the breast surface by adding random errors to the computed temperatures. Also, using four constraint functions, the search area was defined, and within it, the presence of a circular tumor localized at every 1 mm was hypothesized. For each possible tumor position, an auxiliary temperature profile was computed by setting all the tumor thermal properties equal to one. Then the correlation between the simulated temperature distribution and auxiliary temperature profiles was found. The estimated geometric center of the lesion was defined as that that yielded the highest correlation. The authors reported a maximum error for lesion center estimation of 0.32 cm when an invasive lobular carcinoma is located 5 cm underneath the skin surface.

The simulated annealing technique coupled with the dual reciprocity boundary element method was applied by Luna et al. [91] to simultaneously estimate the geometrical (size) and thermophysical (blood perfusion rate and metabolic heat generation) parameters of a breast tumor. The inverse procedure was tested using input temperature data simulated through a bio-heat transfer problem concerning a simplified 2D breast model in which a lesion with different sizes and locations was embedded. The authors underlined that their method does not require the computation of sensitivities or search directions.

To retrieve the radius and location of a spherical tumor in a human breast, Mitra and Balaji [92] applied artificial neural networks in conjunction with the surface temperature distributions computed from a simplified hemispherical finite element breast model. In particular, the studied model considers the breast as a gland with uniform properties. Moreover, to solve the inverse problem, these authors developed a multilayer feed-forward artificial neural network with back propagation learning algorithms using the MATLAB neural network toolbox. This algorithm was trained using the surface temperatures obtained by varying the tumor parameters in the forward problem. The authors reported accuracies of 90% and 95% in the estimation of the position and radius of the tumor, respectively, when no random noise in the temperature data was considered.

A combination of artificial neural networks and genetic algorithms was used by Mital and Pidaparti [93] to prove the possibility of estimating the depth, diameter, and heat generation rates of a breast lesion from simulated surface temperature distributions. In detail, the artificial neural network was trained to provide the temperature distributions of the breast surface as a function of the tumor features, while the genetic algorithm was involved in the estimation procedure. A finite element 2D hemispherical model of the breast described in [94] and consisting of a subcutaneous fat layer, a gland core, a non-uniform muscle layer, and the thoracic wall was used to generate the simulated temperature data. The authors reported good estimation accuracy with low random noise levels.

Saniei et al. [95] applied a trained dynamic neural network model to simultaneously estimate the depth, size, and metabolic heat generation rate of a breast lesion. In particular, the neural network was trained with the results obtained from a 3D finite element model similar to that used in [79]. Contrarily to [93], these authors used real breast thermal images in the estimation procedure. They concluded that the unknown parameters can be determined from a pool of surface temperature data.

7. Post-Processing Images

7.1. Skin Thermograms

An attempt to characterize skin lesions using infrared imaging and image processing was carried out by Shaikh et al. [96]. Using the RGB model, the thermal images were split up into red, green, and blue components. Then, the color frequency was studied using histograms and the K-means segmentation algorithm. An analysis of the results showed that the minimum values of red and green were above 100 and below 100, respectively, while the minimum values of blue were close to zero. The authors concluded that these values can be useful as indicative markers for identifying malignant lesions, or they may be used as thresholds for classification in automated diagnostic systems.

Shaikh et al. [97] used image processing techniques to detect the border of skin cancerous lesions from their thermal images. Different edge detection algorithms, such as Sobel, Canny Edge Detector, Canny-Derliche, and Hysteresis thresholding, were investigated. According to the authors, the Canny Edge Detector and Hysteresis thresholding have the potential to correctly identify the lesion edges. However, the availability of larger databases of skin cancer thermal images is crucial for validating their conclusions.

Benjumea et al. [98] characterized thermographic images of skin lesions through a digital processing procedure involving color segmentation, color tonality-based quantitative discrimination, and analysis by histograms with the aim of identifying the thermal variations in the skin that are indicators of the presence of neoplasms. It is important to underline that thermal images were acquired using the rainbow palette and properly setting the range of temperature measurements so that temperatures higher than 37.5 °C were represented in shades of red. The results highlighted that skin lesions exhibit values in the red component above 100 under the RGB color space on a scale of 0 to 255 [98]. By applying the K-means segmentation algorithm to a thermogram containing a melanoma, the authors noted that the area of the lesion is characterized by a higher average value in the red component compared to the other regions. The authors concluded that, following these results, a detection algorithm for the diagnosis of skin cancer can be developed to reduce unnecessary clinical procedures.

Magalhaes et al. [99] investigated the ability of infrared imaging to identify skin cancer lesions using artificial intelligence algorithms. The authors analyzed a data set of 298 thermograms of malignant and benign lesions to retrieve the thermal parameters to be used as inputs for two machine learning-based strategies, in particular, ensemble learning and deep learning. The deep learning strategy showed the best performances compared to the ensemble learning method (composed of two classifiers: random forest and support vector machine), and it showed good sensitivity and specificity in distinguishing between melanomas/nevi and melanomas/non-melanoma skin cancers. These results prove the potential of IR thermal parameters in the implementation of a diagnostic tool for melanomas detection. However, both tested algorithms did not show good results when non-melanoma skin cancers and benign lesions had to be classified [99]. The authors suggested using the thermal parameters derived from IR thermograms together with dermoscopic images in order to improve the accuracy of the classification method.

7.2. Breast Thermograms

Tang et al. [100] in 2008 suggested a new procedure to detect breast cancer from infrared images based on the measurement of the localized temperature increases. In fact, higher temperature increases in a certain region can lead to a higher possibility that it is

cancerous tissue. In particular, the authors applied a morphological approach to obtain the temperature increase in each image pixel, starting from the definition of a background temperature distribution. By analyzing the thermograms of 117 patients, they found a significant difference between benign and malignant lesions in terms of the maximum temperature increase. Finally, by setting a threshold of 1 °C for the temperature increase, the authors detected 44 of the 47 breast cancer cases.

Zadeh et al. [101] used a combination of genetic algorithms and fuzzy neural networks to analyze the infrared breast images of 200 women, of which only 15 had breast cancer diagnosed by mammography. The authors stated that their method was able to extract the optimal parameters from the thermal images to facilitate an accurate diagnosis, and they also declared a sensitivity of 93%.

A hybrid multiple classifier system to detect breast cancer based on thermal image feature analysis was suggested by Krawczyk and Schaefer [102]. These authors analyzed a data set of 146 breast thermograms, of which 29 were confirmed to be malignant. From these images, they extracted 38 features related to thermal asymmetry between the left and right breast regions. The same features were fed into two different models of classifiers, such as neural networks and support vector machines. To combine the individual classifiers between them, a neural network was used as a trained fuser. Additionally, a fuzzy diversity measurement was defined to eliminate redundant classifiers from the ensemble. The authors stated that their approach not only yields excellent classification accuracy and sensitivity but also outperforms both canonical classification methods.

Mahmoudzadeh et al. [103] suggested a novel extended hidden Markov model to optimize the segmentation process of breast IR images in order to make the analysis of thermal patterns easier. The competitive advantage of their algorithm is its ability to handle random sampling of the IR images without compromising the quality of the segmented images. Moreover, the execution time is reduced compared to other classical image segmentation algorithms, such as Fuzzy C-Means, self-organizing maps, and the standard hidden Markov model.

Recently, Raghavan et al. [104] proposed an improved Generative Adversarial Networks model to produce highly accurate segmentations of breast infrared images. The suggested model was evaluated on three different data sets, yielding high indexes of performance.

Gomathi et al. [105] suggested an unsupervised anisotropic-feature transformation-based classifier for distinguishing normal and abnormal breast thermal images. After image segmentation, statistical features were extracted and used in the classifier. The authors claimed a high level of accuracy when using their procedure.

A convolutional neural network was trained by Ekici and Jawzal [106] for both feature extraction from IR breast images and their successive classification as normal or abnormal thermograms. The authors reported a training accuracy of 97.91% on the data set acquired from 140 subjects. Using the Bayes optimization algorithm, the same accuracy increased up to 98.95%.

Mishra and Rath [107] compared different classifiers, namely support vector machines, decision trees, random forests, K-NN, linear regression, and fuzzy logic, to extract the texture features of 56 breast thermograms. The gray-level run length matrix and gray-level co-occurrence matrix were used for feature extraction. Then the features were selected through unsupervised feature reduction techniques such as principal component analysis and autoencoders. The authors reported that a random forest algorithm coupled with principal component analysis yields an accuracy of 95.45% in classifying healthy and unhealthy breasts.

The performance of two different feature selection methods, namely, Least Absolute Shrinkage and Selection Operator (LASSO) Regression and Adaptive LASSO Regression, was assessed by Mishra et al. [108] when extracting texture characteristics from the breast thermograms. The extracted set of features was classified using support vector machines

with different kernel functions. The authors found that better classification accuracy is obtained when the support vector machine is supported by Adaptive LASSO Regression.

Mahoro and Akhloufi [109] suggested a breast cancer detection system involving a vision-based transformer used for image segmentation and four different convolutional neural network models employed for classification problems, such as EfficientNet-B7, ResNet-50, VGG-16, and DenseNet-201. The authors stated that the best accuracy and sensitivity results were reached using the ResNet-50 model.

A hybrid methodology based on unsupervised and supervised machine learning techniques for analyzing dynamic infrared images was suggested by Silva et al. [110]. Their methodology consists of three main steps. Each recorded image was first divided into a grid of squared pixels, and for each of them, the highest temperature was observed, leading to a temperature time series. Then the k -means clustering algorithm was applied to the set of the obtained time series. After that, clustering validation indices were applied to evaluate the clustering results, and the obtained values were then selected by feature selection algorithms. Finally, the obtained features were fed to different classifier models, such as K-Star, Bayes Net, multi-layer perceptron, decision table, and random forest classification. Although their methodology is able to identify cases of possible cancer with high accuracy, it does not allow the abnormality to be localized in the breast.

Hakim and Awale [111] applied five image segmentation methods to extract the hottest blood vessel patterns from benchmark breast thermograms available in a public data set. The authors concluded that the particle swarm optimization algorithm and multi-seed region-growing technique yield the best segmentation results.

Chebbah et al. [112] suggested a diagnostic tool based on automatic segmentation of breast thermograms. This automatic segmentation was achieved by feeding a deep learning algorithm with 170 infrared breast images. Moreover, to extract relevant features from the segmented thermograms, the authors performed textural evaluation and vascular network analysis. These features were then used as inputs in supervised learning algorithm-based classifiers in order to distinguish between normal and abnormal thermograms. The authors reported very encouraging results for both segmentation and classification.

A deep convolutional neural network with transfer learning was applied by Torres-Galván et al. [113] to automatically classify breast thermograms as normal and abnormal. In particular, they tested the neural network with a group of 311 female subjects. Moreover, two scenarios were considered in the analysis: a balanced class distribution and a typical screening cohort with a low prevalence of abnormal thermograms. The authors reported sensitivity values of 92.3% and 84.6% for the two scenarios, respectively, promoting the use of IR thermography as an adjunct method for breast cancer screening.

8. Conclusions

The renewed interest in IR thermal imaging as a promising technique for the detection of skin and breast cancers, due to the improvement of both IR camera performance and computational capability, has been outlined in the present review. Regarding the thermographic techniques, the following conclusions can be drawn:

- Steady-state thermography is suited to detecting shallower tumors.
- Dynamic thermography can detect deeper tumors using cold/hot stress.
- Lock-in thermography and frequency-modulated thermal wave imaging represent
- New promising methods for the detection of skin lesions.
- Rotational breast thermography has the potential to overcome the limits of conventional breast thermography by allowing the whole breast surface to be analyzed.

Accurate modeling techniques predicting the complex relationship between surface thermal patterns and the underlying pathophysiological conditions represent significant support for the success of this methodology. In particular, an example of these modeling efforts is given by real breast geometry-based models. Moreover, relevant information about thermophysical parameters and growth features of tumor lesions can be inferred from surface temperature distributions using inverse techniques. Data processing algorithms

can help clinicians reach the goal of reducing the number of unnecessary biopsies required for tumor stage characterization.

Lastly, thermogram post-processing methods, especially those based on artificial intelligence algorithms, represent helpful tools for distinguishing between benign and malignant lesions.

In further work, a new review paper should address other clinical applications of IR imaging, such as blood clot imaging.

Author Contributions: Conceptualization, G.D. and S.S.; writing—original draft preparation, G.D.; writing—review and editing, P.T. and S.S.; visualization, G.D.; supervision, P.T. and S.S. All authors have read and agreed to the published version of the manuscript.

Funding: This research received no external funding.

Institutional Review Board Statement: Not applicable.

Informed Consent Statement: Not applicable.

Data Availability Statement: Not applicable.

Conflicts of Interest: The authors declare no conflicts of interest.

References

- World Cancer Research Fund International. Available online: <https://www.wcrf.org> (accessed on 18 December 2023).
- European Cancer Information System (ECIS). Available online: <https://ecis.jrc.ec.europa.eu> (accessed on 18 December 2023).
- Herman, C. Emerging technologies for the detection of melanoma: Achieving better outcomes. *Clin. Cosmet. Investig. Dermatol.* **2012**, *5*, 195–212.
- Akhter, N.; Manza, R.; Shaikh, S.; Gawali, B.; Yannawar, P.; Shaikh, S. Diagnosis of melanoma using thermography: A review. In Proceedings of the International Conference on Applications of Machine Intelligence and Data Analytics (ICAMIDA 2022), Aurangabad, India, 22–24 December 2022. [CrossRef]
- Lahiri, B.B.; Bagavathiappan, S.; Jayakumar, T.; Philip, J. Medical applications of infrared thermography: A review. *Infrared Phys. Technol.* **2012**, *55*, 221–235. [CrossRef] [PubMed]
- Ng, E.Y.K. A review of thermography as promising non-invasive detection modality for breast tumors. *Int. J. Therm. Sci.* **2009**, *48*, 849–859. [CrossRef]
- Lawson, R. Implications of surface temperatures in the diagnosis of breast cancer. *Can. Med. Assoc. J.* **1956**, *75*, 309–310. [PubMed]
- Maillard, G.F.; Hessler, C. La thermographie des melanomes malins cutanes. *Dermatologica* **1969**, *139*, 353–358. [CrossRef] [PubMed]
- Chen, M.M.; Pederson, C.O.; Chato, J.C. On the feasibility of obtaining three dimensional information from thermographic measurements. *J. Biomech. Eng.* **1977**, *99*, 58–64. [CrossRef]
- Cristofolini, M.; Perani, B.; Pisciolli, F.; Recchia, G.; Zumiani, G. Uselessness of thermography for diagnosis and follow-up of cutaneous malignant melanomas. *Tumori* **1981**, *67*, 141–143. [CrossRef]
- Amalric, R.; Altschuler, C.; Giraud, D.; Spitalier, J.M. Value of infrared thermography in the assessment of malignant melanoma of the skin. In *Recent Advances in Medical Thermology*; Ring, E.F.J., Phillips, B., Eds.; Springer: Boston, MA, USA, 1984; pp. 623–629.
- Di Carlo, A. Thermography and the possibilities for its applications in clinical and experimental dermatology. *Clin. Dermatol.* **1995**, *13*, 329–336. [CrossRef]
- Kandlikar, S.G.; Perez-Raya, I.; Raghupathi, P.A.; Gonzalez-Hernandez, J.L.; Dabydeen, D.; Medeiros, L.; Phatak, P. Infrared imaging technology for breast cancer detection—Current status, protocols and new directions. *Int. J. Heat Mass Transf.* **2017**, *108*, 2303–2320. [CrossRef]
- Mashekova, A.; Zhao, Y.; Ng, E.Y.K.; Zarikas, V.; Fok, S.C.; Mukhmetov, O. Early detection of the breast cancer using infrared technology—A comprehensive review. *Therm. Sci. Eng. Prog.* **2022**, *27*, 101142. [CrossRef]
- Verstockt, J.; Verspeek, S.; Thiessen, F.; Tjalma, W.A.; Brochez, L.; Steenackers, G. Skin cancer detection using infrared thermography: Measurement setup, procedure and equipment. *Sensors* **2022**, *22*, 3327. [CrossRef] [PubMed]
- González, F.J.; Castillo-Martínez, C.; Valdes-Rodríguez, R.; Kolosovas-Machuca, E.S.; Villela-Segura, U.; Moncada, B. Thermal signature of melanoma and non-melanoma skin cancers. In Proceedings of the 11th International Conference on Quantitative InfraRed Thermography QIRT 2012, Naples, Italy, 11–14 June 2012.
- Head, J.F.; Wang, F.; Lipari, C.A.; Elliott, R.L. The important role of infrared imaging in breast cancer. *IEEE Eng. Med. Biol.* **2000**, *19*, 52–57. [CrossRef] [PubMed]
- Figueiredo, A.A.A.; do Nascimento, J.G.; Malheiros, F.C.; da Silva Ignacio, L.H.; Fernandes, H.C.; Guimaraes, G. Breast tumor localization using skin surface temperatures from a 2D anatomic model without knowledge of the thermophysical properties. *Comput. Methods Programs Biomed.* **2019**, *172*, 65–77. [CrossRef] [PubMed]

19. Yahara, T.; Koga, T.; Yoshida, S.; Nakagawa, S.; Deguchi, H.; Shirouzu, K. Relationship between microvessel density and thermography hot areas in breast cancer. *Surg. Today* **2003**, *33*, 243–248. [[PubMed](#)]
20. Francis, S.V.; Sasikala, M.; Bharathi, G.B.; Jaipurkar, S.D. Breast cancer detection in rotational thermography images using texture features. *Infrared Phys. Technol.* **2014**, *67*, 490–496. [[CrossRef](#)]
21. Keyserlingk, J.R.; Ahlgren, P.D.; Yu, E.; Belliveau, N. Infrared imaging of the breast: Initial reappraisal using high-resolution digital technology in 100 successive cases of stage I and II breast cancer. *Breast J.* **1998**, *4*, 245–251. [[CrossRef](#)] [[PubMed](#)]
22. Gershenson, M.; Gershenson, J. Dynamic vascular imaging using active breast thermography. *Sensors* **2023**, *23*, 3012. [[CrossRef](#)] [[PubMed](#)]
23. Buzug, T.M.; Schumann, S.; Pfaffmann, L.; Reinhold, U.; Ruhlmann, J. Functional infrared imaging for skin-cancer screening. In Proceedings of the 28th Annual International Conference of the IEEE Engineering in Medicine and Biology Society EMBS'06, New York, NY, USA, 30 August–3 September 2006.
24. Solivetti, F.M.; Desiderio, F.; Guerrisi, A.; Bonadies, A.; Maini, C.L.; Di Filippo, S.; D'Orazi, V.; Sperduti, I.; Di Carlo, A. HF ultrasound vs PET-CT and telethermography in the diagnosis of In-transit metastases from melanoma: A prospective study and review. *J. Exp. Clin. Cancer Res.* **2014**, *33*, 96. [[CrossRef](#)]
25. Magalhaes, C.; Vardasca, R.; Rebelo, M.; Valenca-Filipe, R.; Ribeiro, M.; Mendes, J. Distinguishing melanocytic nevi from melanomas using static and dynamic infrared thermal imaging. *J. Eur. Acad. Dermatol. Venereol.* **2019**, *33*, 1700–1705. [[CrossRef](#)]
26. Flores-Sahagun, J.H.; Vargas, J.V.C.; Mulinari-Brenner, F.A. Analysis and diagnosis of basal cell carcinoma (BCC) via infrared imaging. *Infrared Phys. Technol.* **2011**, *54*, 367–378. [[CrossRef](#)]
27. Vargas, J.V.C.; Brioschi, M.L.; Dias, F.G.; Parolin, M.B.; Mulinari-Brenner, F.A.; Ordonez, J.C.; Colman, D. Normalized methodology for medical infrared imaging. *Infrared Phys. Technol.* **2009**, *52*, 42–47. [[CrossRef](#)]
28. Shada, A.L.; Dengel, L.T.; Petroni, G.R.; Smolkin, M.E.; Acton, S.; Slingluff, C.L., Jr. Infrared thermography of cutaneous melanoma metastases. *J. Surg. Res.* **2013**, *182*, e9–e14. [[CrossRef](#)] [[PubMed](#)]
29. Vardasca, R.; Esteves, L.; Rebelo, M.; Gabriel, J. Malignant melanoma characterization with thermal and visual imaging. In *Infrared Imaging a Casebook in Clinical Medicine*; Ring, A., Jung, A., Zuber, J., Eds.; IOP Publishing: Bristol, UK, 2015; pp. 9–1–9–3.
30. Stringasci, M.D.; Salvio, A.G.; Sbrissa Neto, D.; Vollet-Filho, J.D.; Bagnato, V.S.; Kurachi, C. Discrimination of benign-versus malignant skin lesions by thermographic images using support vector machine classifier. *J. Appl. Phys.* **2018**, *124*, 044701-1–044701-8. [[CrossRef](#)]
31. Zenzie, H.H.; Altshuler, G.B.; Smirnov, M.Z.; Anderson, R.R. Evaluation of cooling methods for laser dermatology. *Lasers Surg. Med.* **2000**, *26*, 130–144. [[CrossRef](#)]
32. Deng, Z.S.; Liu, J. Enhancement of thermal diagnostics on tumors underneath the skin by induced evaporation. In Proceedings of the 27th Annual Conference of IEEE Engineering in Medicine and Biology, Shanghai, China, 1–4 September 2005.
33. Cheng, T.Y.; Herman, C. Analysis of skin cooling for quantitative dynamic infrared imaging of near-surface lesions. *Int. J. Therm. Sci.* **2014**, *86*, 175–188. [[CrossRef](#)]
34. Gomboc, T.; Iljaž, J.; Wrobel, L.C.; Hriberšek, M.; Marn, J. Design of constant temperature cooling device for melanoma screening by dynamic thermography. *Eng. Anal. Bound. Elem.* **2021**, *125*, 66–79. [[CrossRef](#)]
35. Verstockt, J.; Thiessen, F.E.F.; Hoorens, I.; Brochez, L.; Steenackers, G. Comparative analysis of cooling methods for dynamic infrared thermography (DIRT)-based skin cancer diagnosis. *Appl. Sci.* **2023**, *13*, 10105. [[CrossRef](#)]
36. Verstockt, J.; Somers, R.; Thiessen, F.E.F.; Hoorens, I.; Brochez, L.; Steenackers, G. Finite element skin models as additional data for dynamic infrared thermography on skin lesions. *Quant. InfraRed Thermogr. J.* **2023**. [[CrossRef](#)]
37. Santa Cruz, G.A.; Bertotti, J.; Marin, J.; Gonzalez, S.J.; Gossio, S.; Alvarez, D.; Roth, B.M.C.; Menendez, P.; Pereira, M.D.; Albero, M.; et al. Dynamic infrared imaging of cutaneous melanoma and normal skin in patients treated with BNCT. *Appl. Radiat. Isot.* **2009**, *67*, S54–S58. [[CrossRef](#)]
38. Cetingul, M.P.; Herman, C. The assessment of melanoma risk using the dynamic infrared imaging technique. *J. Therm. Sci. Eng. Appl.* **2011**, *3*, 031006-1–031006-9. [[CrossRef](#)]
39. Di Carlo, A.; Elia, F.; Desiderio, F.; Catricalà, C.; Solivetti, F.M.; Laino, L. Can video thermography improve differential diagnosis and therapy between basal cell carcinoma and actinic keratosis? *Dermatol. Ther.* **2014**, *27*, 290–297. [[CrossRef](#)]
40. Baek, Y.S.; Kim, A.; Seo, J.Y.; Jeon, J.; Oh, C.H.; Kim, J. Dynamic thermal imaging for pigmented basal cell carcinoma and seborrheic keratosis. *Int. J. Hyperth.* **2021**, *38*, 1462–1468. [[CrossRef](#)]
41. Godoy, S.E.; Ramirez, D.A.; Myers, S.A.; von Winckel, G.; Krishna, S.; Berwick, M.; Padilla, R.S.; Sen, P.; Krishna, S. Dynamic infrared imaging for skin cancer screening. *Infrared Phys. Technol.* **2015**, *70*, 147–152. [[CrossRef](#)]
42. Laino, L.; Elia, F.; Desiderio, F.; Scarabello, A.; Sperduti, I.; Cota, C.; Di Carlo, A. The efficacy of a photolyase-based device on the cancerization field: A clinical and thermographic study. *J. Exp. Clin. Cancer Res.* **2015**, *34*, 84. [[CrossRef](#)] [[PubMed](#)]
43. Cholewka, A.; Stanek, A.; Kwiatek, S.; Cholewka, A.; Cieslar, G.; Straszak, D.; Gibinska, J.; Sieron-Stożny, K. Proposal of thermal imaging application in photodynamic therapy—Preliminary report. *Photodiagn. Photodyn. Ther.* **2016**, *14*, 34–39. [[CrossRef](#)] [[PubMed](#)]
44. Bonmarin, M.; Le Gal, F.-A. A lock-in thermal imaging setup for dermatological applications. *Ski. Res. Technol.* **2015**, *21*, 284–290. [[CrossRef](#)] [[PubMed](#)]
45. Bhowmik, A.; Repaka, R.; Mulaveesala, R.; Mishra, S.C. Suitability of frequency modulated thermal wave imaging for skin cancer detection—A theoretical prediction. *J. Therm. Biol.* **2015**, *51*, 65–82. [[CrossRef](#)]

46. Ohashi, Y.; Uchida, I. Applying dynamic thermography in the diagnosis of breast cancer. *IEEE Eng. Med. Biol.* **2000**, *19*, 42–51. [[CrossRef](#)]
47. Vreugdenburg, T.D.; Willis, C.D.; Mundy, L.; Hiller, J.E. A systematic review of elastography, electrical impedance scanning, and digital infrared thermography for breast cancer screening and diagnosis. *Breast Cancer Res. Treat.* **2013**, *137*, 665–676. [[CrossRef](#)]
48. Ng, E.Y.K.; Chen, Y.; Ung, L.N. Computerized breast thermography: Study of image segmentation and temperature cyclic variations. *J. Med. Eng. Technol.* **2001**, *25*, 12–16.
49. Zeng, J.; Lin, L.; Deng, F. Infrared thermal imaging as a nonradiation method for detecting thermal expression characteristics in normal female breasts in China. *Infrared Phys. Technol.* **2020**, *104*, 103125. [[CrossRef](#)]
50. Wang, Y.; Chang, K.J.; Chen, C.Y.; Chien, K.L.; Tsai, Y.S.; Wu, Y.M.; Teng, Y.C.; Shih, T.T.F. Evaluation of the diagnostic performance of infrared imaging of the breast: A preliminary study. *Biomed. Eng. Online* **2010**, *9*, 3. [[CrossRef](#)] [[PubMed](#)]
51. Kontos, M.; Wilson, R.; Fentiman, I. Digital infrared thermal imaging (DITI) of breast lesions: Sensitivity and specificity of detection of primary breast cancers. *Clin. Radiol.* **2011**, *66*, 536–539. [[CrossRef](#)] [[PubMed](#)]
52. Morais, K.C.C.; Vargas, J.V.C.; Reiserberger, G.G.; Freitas, F.N.P.; Oliari, S.H.; Brioschi, M.L.; Louveira, M.H.; Spautz, C.; Dias, F.G.; Gasperin, P., Jr.; et al. An infrared image based methodology for breast lesions screening. *Infrared Phys. Technol.* **2016**, *76*, 710–721.
53. Amri, A.; Pulko, S.H.; Wilkinson, A.J. Potentialities of steady-state and transient thermography in breast tumour depth detection: A numerical study. *Comput. Methods Programs Biomed.* **2016**, *123*, 68–80. [[CrossRef](#)] [[PubMed](#)]
54. Zhou, Y.; Herman, C. Optimization of skin cooling by computational modeling for early thermographic detection of breast cancer. *Int. J. Heat Mass Transf.* **2018**, *126*, 864–876. [[CrossRef](#)]
55. Sadeghi, M.; Boese, A.; Maldonado, I.; Sauerhering, J.; Schlosser, S.; Wehberg, H.; Wehberg, K.; Friebe, M. Feasibility test of dynamic cooling for detection of small tumors in IR thermographic breast imaging. *Curr. Dir. Biomed. Eng.* **2019**, *5*, 397–400. [[CrossRef](#)]
56. Parisky, Y.R.; Sardi, A.; Hamm, R.; Hughes, K.; Esserman, L.; Rust, S.; Callahan, K. Efficacy of computerized infrared imaging analysis to evaluate mammographically suspicious lesions. *Am. J. Roentgenol.* **2003**, *180*, 263–269. [[CrossRef](#)]
57. Arora, N.; Martins, D.; Ruggerio, D.; Tousimis, E.; Swistel, A.J.; Osborne, M.P.; Simmons, R.M. Effectiveness of a noninvasive digital infrared thermal imaging system in the detection of breast cancer. *Am. J. Surg.* **2008**, *196*, 523–526. [[CrossRef](#)]
58. Wishart, G.C.; Campisi, M.; Boswell, M.; Chapman, D.; Shackleton, V.; Iddles, S.; Hallett, A.; Britton, P.D. The accuracy of digital infrared imaging for breast cancer detection in women undergoing breast biopsy. *EJSO Eur. J. Surg. Oncol.* **2010**, *36*, 535–540. [[CrossRef](#)]
59. Sarigoz, T.; Ertan, T. Role of dynamic thermography in diagnosis of nodal involvement in patients with breast cancer: A pilot study. *Infrared Phys. Technol.* **2020**, *108*, 103336. [[CrossRef](#)]
60. Deng, Z.-S.; Liu, J. Mathematical modeling of temperature mapping over skin surface and its implementation in thermal disease diagnostics. *Comput. Biol. Med.* **2004**, *34*, 495–521. [[CrossRef](#)] [[PubMed](#)]
61. Cetingul, M.P.; Herman, C. A heat transfer model of skin tissue for the detection of lesions: Sensitivity analysis. *Phys. Med. Biol.* **2010**, *55*, 5933–5951. [[CrossRef](#)] [[PubMed](#)]
62. Cetingul, M.P.; Herman, C. Quantification of the thermal signature of a melanoma lesion. *Int. J. Therm. Sci.* **2011**, *50*, 421–431. [[CrossRef](#)]
63. Bhowmik, A.; Repaka, R.; Mishra, S.C. Thermographic evaluation of early melanoma within the vascularized skin using combined non-Newtonian blood flow and bio heat models. *Comput. Biol. Med.* **2014**, *53*, 206–219. [[CrossRef](#)] [[PubMed](#)]
64. Bonmarin, M.; Le Gal, F.-A. Lock-in thermal imaging for the early-stage detection of cutaneous melanoma: A feasibility study. *Comput. Biol. Med.* **2014**, *47*, 36–43. [[CrossRef](#)] [[PubMed](#)]
65. Iljaž, J.; Wrobel, L.C.; Hriberšek, M.; Marn, J. Subdomain BEM formulations for the solution of bio-heat problems in biological tissue with melanoma lesions. *Eng. Anal. Bound. Elem.* **2017**, *83*, 25–42. [[CrossRef](#)]
66. Agyingi, E.; Wiandt, T.; Maggelakis, S. A quantitative model of cutaneous melanoma diagnosis using thermography. In *Mathematical and Computational Approaches in Advancing Modern Science and Engineering*; Bélair, J., Frigaard, I.A., Kunze, H., Makarov, R., Melnik, R., Spiteri, R.J., Eds.; Springer: Cham, Switzerland, 2016; pp. 167–175. [[CrossRef](#)]
67. Greene, F.L.; Compton, C.C.; Fritz, A.G.; Shah, J.P.; Winchester, D.P. Melanoma of the Skin. In *AJCC Cancer Staging Atlas, Part V*; Greene, F.L., Compton, C.C., Fritz, A.G., Shah, J.P., Winchester, D.P., Eds.; Springer: New York, NY, USA, 2006; pp. 207–216.
68. Partridge, P.W.; Wrobel, L.C. An inverse geometry problem for the localisation of skin tumours by thermal analysis. *Eng. Anal. Bound. Elem.* **2007**, *31*, 803–811. [[CrossRef](#)]
69. Agnelli, J.P.; Barrea, A.A.; Turner, C.V. Tumor location and parameter estimation by thermography. *Math. Comput. Model.* **2011**, *53*, 1527–1534. [[CrossRef](#)]
70. Bhowmik, A.; Repaka, R. Estimation of growth features and thermophysical properties of melanoma within 3D human skin using genetic algorithm and simulated annealing. *Int. J. Heat Mass Transf.* **2016**, *98*, 81–95. [[CrossRef](#)]
71. Strakowska, M.; Strakowski, R.; Strzelecki, M.; de Mey, G.; Więcek, B. Evaluation of perfusion and thermal parameters of skin tissue using cold provocation and thermographic measurements. *Metrol. Meas. Syst.* **2016**, *23*, 373–381. [[CrossRef](#)]
72. Strakowska, M.; Strakowski, R.; Strzelecki, M.; de Mey, G.; Więcek, B. Thermal modelling and screening method for skin pathologies using active thermography. *Biocybern. Biomed. Eng.* **2018**, *38*, 602–610. [[CrossRef](#)]

73. Iljaž, J.; Wrobel, L.C.; Gomboc, T.; Hriberšek, M.; Marn, J. Solving inverse bioheat problems of skin tumour identification by dynamic thermography. *Inverse Probl.* **2020**, *36*, 035002. [[CrossRef](#)]
74. Iljaž, J.; Wrobel, L.C.; Hriberšek, M.; Marn, J. Numerical modelling of skin tumour tissue with temperature-dependent properties for dynamic thermography. *Comput. Biol. Med.* **2019**, *112*, 103367. [[CrossRef](#)] [[PubMed](#)]
75. Iljaž, J.; Wrobel, L.C.; Hriberšek, M.; Marn, J. The use of Design of Experiments for steady-state and transient inverse melanoma detection problems. *Int. J. Therm. Sci.* **2019**, *135*, 256–275. [[CrossRef](#)]
76. Chen, H.; Wang, K.; Du, Z.; Liu, W.; Liu, Z. Predicting the thermophysical properties of skin tumor based on the surface temperature and deep learning. *Int. J. Heat Mass Transf.* **2021**, *180*, 121804. [[CrossRef](#)]
77. Jiang, L.; Zhan, W.; Loew, M.H. Modeling static and dynamic thermography of the human breast under elastic deformation. *Phys. Med. Biol.* **2011**, *56*, 187–202. [[CrossRef](#)] [[PubMed](#)]
78. Mukhmetov, O.; Igali, D.; Mashekova, A.; Zhao, Y.; Ng, E.Y.K.; Fok, S.C.; Teh, S.L. Thermal modeling for breast tumor detection using thermography. *Int. J. Therm. Sci.* **2021**, *161*, 106712. [[CrossRef](#)]
79. Ng, E.Y.K.; Sudharsan, N.M. Effect of blood flow, tumour and cold stress in a female breast: A novel time-accurate computer simulation. *Proc. Inst. Mech. Eng. Part H J. Eng. Med.* **2001**, *215*, 393–404. [[CrossRef](#)]
80. Lozano, A.; Hayes, J.C.; Compton, L.M.; Azarnoosh, J.; Hassanipour, F. Determining the thermal characteristics of breast cancer based on high-resolution infrared imaging, 3D breast scans, and magnetic resonance imaging. *Sci. Rep.* **2020**, *10*, 10105. [[CrossRef](#)]
81. Amri, A.; Saidane, A.; Pulkko, S. Thermal analysis of a three-dimensional breast model with embedded tumour using the transmission line matrix (TLM) method. *Comput. Biol. Med.* **2011**, *41*, 76–86. [[CrossRef](#)] [[PubMed](#)]
82. Wahab, A.A.; Salim, M.I.M.; Ahamat, M.A.; Manaf, N.A.; Yunus, J.; Lai, K.W. Thermal distribution analysis of three-dimensional tumor-embedded breast models with different breast density compositions. *Med. Biol. Eng. Comput.* **2016**, *54*, 1363–1373. [[CrossRef](#)] [[PubMed](#)]
83. Al Husaini, M.A.S.; Habaebi, M.H.; Suliman, F.M.; Islam, R.; Elsheikh, E.A.A.; Muhaisen, N.A. Influence of tissue thermophysical characteristics and situ-cooling on the detection of breast cancer. *Appl. Sci.* **2023**, *13*, 8752. [[CrossRef](#)]
84. Paruch, M.; Majchrzak, E. Identification of tumor region parameters using evolutionary algorithm and multiple reciprocity boundary element method. *Eng. Appl. Artif. Intell.* **2007**, *20*, 647–655. [[CrossRef](#)]
85. Das, K.; Mishra, S.C. Simultaneous estimation of size, radial and angular locations of a malignant tumor in a 3-D human breast—A numerical study. *J. Therm. Biol.* **2015**, *52*, 147–156. [[CrossRef](#)] [[PubMed](#)]
86. Das, K.; Mishra, S.C. Non-invasive estimation of size and location of a tumor in a human breast using a curve fitting technique. *Int. Commun. Heat Mass Transf.* **2014**, *56*, 63–70. [[CrossRef](#)]
87. Hossain, S.; Mohammadi, F.A. Tumor parameter estimation considering the body geometry by thermography. *Comput. Biol. Med.* **2016**, *76*, 80–93. [[CrossRef](#)]
88. Ferreira de Melo, J.R.; Queiroz, J.R.A.; Bezerra, L.A.; de Lima, R.C.F. Development of a three-dimensional surrogate geometry of the breast and its use in estimating the thermal conductivities of breast tissue and breast lesions based on infrared images. *Int. Commun. Heat Mass Transf.* **2019**, *108*, 104279. [[CrossRef](#)]
89. Bezerra, L.A.; Oliveira, M.M.; Rolim, T.L.; Conci, A.; Santos, F.G.S.; Lyra, P.R.M.; Lima, R.C.F. Estimation of breast tumor thermal properties using infrared images. *Signal Process.* **2013**, *93*, 2851–2863. [[CrossRef](#)]
90. Hatwar, R.; Herman, C. Inverse method for quantitative characterization of breast tumours from surface temperature data. *Int. J. Hyperth.* **2017**, *33*, 741–757.
91. Luna, J.M.; Romero-Mendez, R.; Hernandez-Guerrero, A.; Elizalde-Blancas, F. Procedure to estimate thermophysical and geometrical parameters of embedded cancerous lesions using thermography. *J. Biomech. Eng.* **2012**, *134*, 031008.
92. Mitra, S.; Balaji, C. A neural network based estimation of tumour parameters from a breast thermogram. *Int. J. Heat Mass Transf.* **2010**, *53*, 4714–4727. [[CrossRef](#)]
93. Mital, M.; Pidaparti, R.M. Breast tumor simulation and parameters estimation using evolutionary algorithms. *Model. Simul. Eng.* **2008**, *2008*, 756436. [[CrossRef](#)]
94. Sudarshan, N.M.; Ng, E.Y.K.; Teh, S.L. Surface temperature distribution of a breast with and without tumour. *Comput. Methods Biomech. Biomed. Eng.* **1999**, *2*, 187–199. [[CrossRef](#)] [[PubMed](#)]
95. Saniei, E.; Setayeshi, S.; Akbari, M.E.; Navid, M. Parameter estimation of breast tumour using dynamic neural network from thermal pattern. *J. Adv. Res.* **2016**, *7*, 1045–1055. [[CrossRef](#)] [[PubMed](#)]
96. Shaikh, S.; Akhter, N.; Manza, R. Application of image processing techniques for characterization of skin cancer lesions using thermal images. *Indian J. Sci. Technol.* **2016**, *9*, 1–7. [[CrossRef](#)]
97. Shaikh, S.; Akhter, N.; Gaike, V.; Manza, R. Boundary detection of skin cancer lesions using image processing techniques. *J. Med. Chem. Drug Discov.* **2016**, *1*, 381–388.
98. Benjumea, E.; Morales, Y.; Torres, C.; Vildary, J. Characterization of thermographic images of skin cancer lesions using digital image processing. In Proceedings of the IX International Congress of Physics Engineering, Mexico City, Mexico, 5–9 November 2018.
99. Magalhaes, C.; Tavares, J.M.R.S.; Mendes, J.; Vardasca, R. Comparison of machine learning strategies for infrared thermography of skin cancer. *Biomed. Signal Process. Control* **2021**, *69*, 102872. [[CrossRef](#)]
100. Tang, X.; Ding, H.; Yuan, Y.; Wang, Q. Morphological measurement of localized temperature increase amplitudes in breast infrared thermograms and its clinical application. *Biomed. Signal Process. Control* **2008**, *3*, 312–318. [[CrossRef](#)]

101. Zadeh, H.G.; Pakdelazar, O.; Haddadnia, J.; Rezaei-Rad, G.; Mohammad-Zadeh, M. Diagnosing breast cancer with the aid of fuzzy logic based on data mining of a genetic algorithm in infrared images. *Middle East J. Cancer* **2011**, *3*, 119–129.
102. Krawczyk, B.; Schaefer, G. A hybrid classifier committee for analysing asymmetry features in breast thermograms. *Appl. Soft Comput.* **2014**, *20*, 112–118. [[CrossRef](#)]
103. Mahmoudzadeh, E.; Montazeri, M.A.; Zekri, M.; Sadri, S. Extended hidden Markov model for optimized segmentation of breast thermography images. *Infrared Phys. Technol.* **2015**, *72*, 19–28. [[CrossRef](#)]
104. Raghavan, K.; Balasubramanian, S.; Veezhinathan, K. IR-GAN: Improved generative adversarial networks for infrared breast image segmentation. *Quant. InfraRed Thermogr. J.* **2023**, *in press*. [[CrossRef](#)]
105. Gomathi, P.; Muniraj, C.; Periasamy, P.S. Breast thermography based unsupervised anisotropic- feature transformation method for automatic breast cancer detection. *Microprocess. Microsyst.* **2020**, *77*, 103137. [[CrossRef](#)]
106. Ekici, S.; Jawzal, H. Breast cancer diagnosis using thermography and convolutional neural networks. *Med. Hypotheses* **2020**, *137*, 109542. [[CrossRef](#)]
107. Mishra, V.; Rath, S.K. Detection of breast cancer tumours based on feature reduction and classification of thermograms. *Quant. InfraRed Thermogr. J.* **2021**, *18*, 300–313. [[CrossRef](#)]
108. Mishra, V.; Rath, S.K.; Mohapatra, D.P. Thermograms-based detection of cancerous tumors in breasts applying texture features. *Quant. InfraRed Thermogr. J.* **2023**, *in press*. [[CrossRef](#)]
109. Mahoro, E.; Akhloufi, M.A. Breast cancer classification on thermograms using deep CNN and transformers. *Quant. InfraRed Thermogr. J.* **2024**, *21*, 30–49. [[CrossRef](#)]
110. Silva, L.F.; Santos, A.A.S.M.D.; Bravo, R.S.; Silva, A.C.; Muchaluat-Saadea, D.C.; Conci, A. Hybrid analysis for indicating patients with breast cancer using temperature time series. *Comput. Methods Programs Biomed.* **2016**, *130*, 142–153. [[CrossRef](#)]
111. Hakim, A.S.; Awale, R.N. Extraction of hottest blood vessels from breast thermograms using state-of-the-art image segmentation methods. *Quant. InfraRed Thermograms. J.* **2022**, *19*, 347–365. [[CrossRef](#)]
112. Chebbah, N.K.; Ouslim, M.; Benabid, S. New computer aided diagnostic system using deep neural network and SVM to detect breast cancer in thermography. *Quant. InfraRed Thermogr. J.* **2023**, *20*, 62–77. [[CrossRef](#)]
113. Torres-Galván, J.C.; Guevara, E.; Kolosovas-Machuca, E.S.; Ocegüera-Villanueva, A.; Flores, J.L.; González, F.J. Deep convolutional neural networks for classifying breast cancer using infrared thermography. *Quant. InfraRed Thermogr. J.* **2022**, *19*, 283–294. [[CrossRef](#)]

Disclaimer/Publisher’s Note: The statements, opinions and data contained in all publications are solely those of the individual author(s) and contributor(s) and not of MDPI and/or the editor(s). MDPI and/or the editor(s) disclaim responsibility for any injury to people or property resulting from any ideas, methods, instructions or products referred to in the content.